CHEMISTRY OF MATERIALS

pubs.acs.org/cm

Perspective

Imperfect Battery Materials: A Closer Look at the Role of Defects in Electrochemical Performance

Marine Reynaud,[▽] Jon Serrano-Sevillano,[▽] and Montse Casas-Cabanas*

Cite This: *Chem. Mater.* 2023, 35, 3345−3363

Read Online

ACCESS | Metrics & More | Article Recommendations

ABSTRACT: Structural and compositional defects in crystalline materials are unavoidable. Accurately disentangling their role in composition−structure−property correlations is therefore essential but has long been hindered by our inability to precisely identify and quantify certain microstructural features. As a result, deviations from ideal structures have frequently been disregarded or assumed to be detrimental. Nonetheless, today's structural disorder characterization advancements offer unprecedented insights into defect architectures. Recent models and tools applied to scattering and spectroscopic techniques provide an accessible window for observing and accurately parametrizing microstructural complexity and, if understood and mastered, offer the utmost control for designing better materials. One important field that can greatly benefit from advancement in the understanding and control of structural defects is the development of battery materials, whose performance and cycle life are closely related to structural aspects, including defects. This perspective offers an overview of the progress achieved in this field, with a special focus on cathode materials, and a discussion about opportunities for future developments.

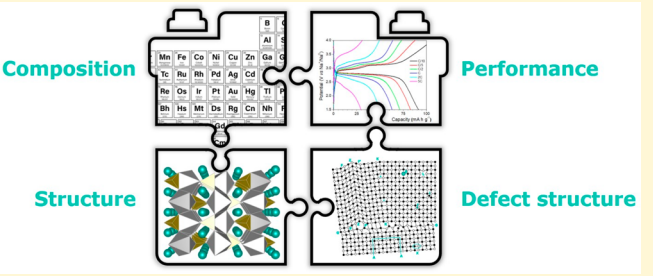

INTRODUCTION

Solids are usually classified into two categories depending on the arrangement of their atomic constituents: (i) *amorphous* compounds, where the arrangement of the atoms in the solid does not follow any regular pattern at long-range, and (ii) *crystalline* compounds, where the atoms are arranged according to a lattice pattern that is periodically repeated along the three directions of the space. This periodicity in crystalline solids is often thought of (and taught) as being perfect. However, perfect crystals are very often oversimplified ideal models, as these could only exist at absolute zero temperature. Imperfections are a universal feature of crystalline materials, and these irregularities can profoundly affect macroscopic physical properties and chemical reactivity. Ideal infinite periodic structural models are thus precious tools to establish many of the structure−property correlations in solids, but they are sometimes insufficient.

Although the relevance of imperfections has long been recognized in several fields, they are still often disregarded or oversimplified. To begin with, imperfections in crystalline solids are often referred to as *defects*. This word usually carries a distinctly negative connotation and might erroneously bring to mind that their presence is detrimental to performance. As a result, such mistaken appreciation can foster considerable efforts to either minimize their concentration or counterbalance their impact. Conversely, defects in solids can generate value.[1,2] *Point defects* and *impurities* cause highly desirable colors in gem-quality diamonds and other precious stones.[3] *Dopants*, which is a more attractive name to refer to purposely introduced *chemical impurities*, constitute the foundation of the entire semiconductor industry, which masters methods to precisely insert tiny amounts of desired impurities into Si, Ge, or GaAs to finely tune the electrical conductivity. *Chemical substitutions* are also used in battery materials, for instance, as a tool to enhance ionic conductivity in ceramic electrolytes with *isovalent* and *aliovalent substitutions*,[4,5] to modify the reaction mechanism and smoothen the voltage profile of insertion electrode materials with *doping*,[6] or to tune the redox potentials of their redox centers thanks to *cationic/metal and anionic substitutions*.[7,8] *Linear defects* such as *dislocations* have a relevant role in plastic deformations in metallurgy.[9] Conversely, their role in battery materials is still largely underexplored. Yet, a few papers suggest that dislocations may provide an energetically favorable diffusion path for the diffusion of mobile ions, relieve lattice strain during phase transformations and prevent particle cracking, or participate through motion of dislocations in the layer gliding mechanism occurring in the phase transformation(s) of layered battery materials upon

Received: November 22, 2022
Revised: February 17, 2023
Published: March 22, 2023

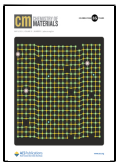

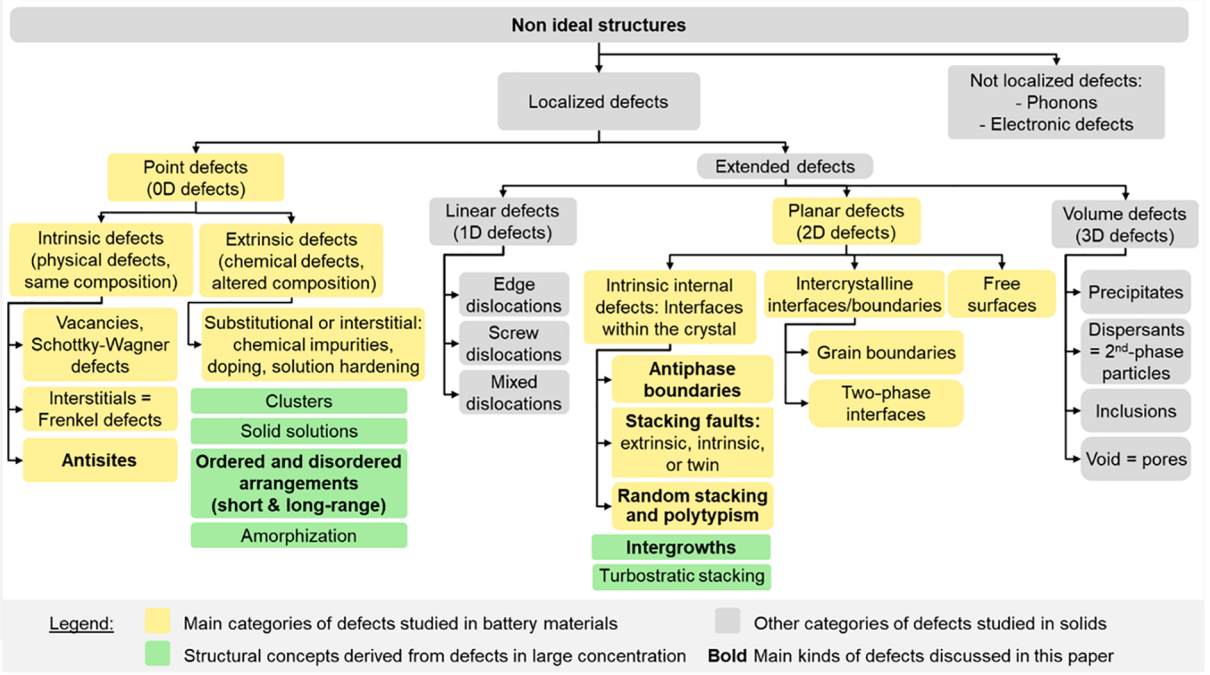

Figure 1. Different categories of defects found in crystalline solids. The two main categories of defects (point defects and planar defects) that have been investigated in battery materials are highlighted in yellow. Structural concepts derived from defects in large concentrations are shown in green. The main kinds of defects discussed in this paper are highlighted in bold.

alkali (de)intercalation.[10] *Planar defects* such as *twin boundaries* give rise to the peculiar shapes of twinned crystals of minerals. The presence of *grain boundaries* separating small crystallites or grains prevents the motion of dislocations and hence strengthens the material. For solid-state battery applications, however, electrolytes are often annealed to recrystallize the polycrystalline materials with the aim to favor ionic mobility within the bulk and to avoid Li dendrite propagation within *grain boundaries* and volume defects such as *cracks*, *voids*, and *pores*.[11,12]

On the other hand, defects have also been repeatedly ignored in the evaluation of structure−property correlations because achieving a complete, quantitative, and accurate description often represents a challenge. This is due to several factors. First, defects can be detected with a limited number of characterization methods, which can be defect-specific and in general are still not widely applied. Next, crystal structures are extraordinarily diverse (as are the defect structures resulting from different synthetic conditions and combinations of defects), and these might even dynamically evolve (e.g., phase transformations). The intentional introduction of defects (with control over the type, concentration, location, etc.) thus offers an exciting research avenue for materials design and engineering.

Battery materials are representative of the significant and far-reaching benefits of seizing this opportunity. Innovation through structural design has been an effective means for the realization of today's batteries. Our ability to master the atomic scale through the identification of host structures and chemistries able to intercalate lithium ions at convenient voltages has been rewarded by the deployment of Li-ion technology and the ushering in of the portable electronics era. However, improving battery materials' performances, using the same earth-abundant elements, now requires a more complete understanding of the thermodynamic and kinetic phenomena occurring across all relevant length scales. Our ability to precisely describe both the structure and the microstructure (including the defect structure) is essential in this context.

In this Perspective, we discuss the potential of such approaches. First, an overview of the main types of defects studied in battery materials is provided, then we review the effect of intrinsic-type defects on the electrochemical performance of a selection of electrode and electrolyte materials. Whether these are detrimental or represent an enhancement of the material function needs to be analyzed case by case, as shown here. We then examine how the latest advances in characterization methodologies and the understanding of microstructural defects in these materials have opened new ways for designing battery materials with improved performance. Finally, building on this knowledge, we identify several exciting opportunities to conduct additional research in this field.

MAIN TYPES OF DEFECTS IN BATTERY MATERIALS

A *defect* can be defined as an alteration of the configuration of the (atomic or electronic) structure of the ideal solid. The different categories of defects that are encountered in crystalline solids are described in Figure 1. Listing an exhaustive, detailed description of each of these defects is out of the scope of this Perspective. For this purpose, the reader can refer to many books dedicated to the fundamentals of materials science that include chapters focused on defects, such as refs 13 and 14. The main kinds of defects that have been investigated in battery materials are highlighted in yellow in Figure 1, and most of them are illustrated in Figure 2. They can be gathered into two main categories: *point defects* and *planar defects*; they are further described below.

Point defects consist of zero-dimensional irregularities in the crystal structure and are usually divided into two groups (although they might appear combined): *intrinsic point defects*, which are physical defects and therefore do not involve foreign elements, and *extrinsic*

https://doi.org/10.1021/acs.chemmater.2c03481
Chem. Mater. 2023, 35, 3345−3363

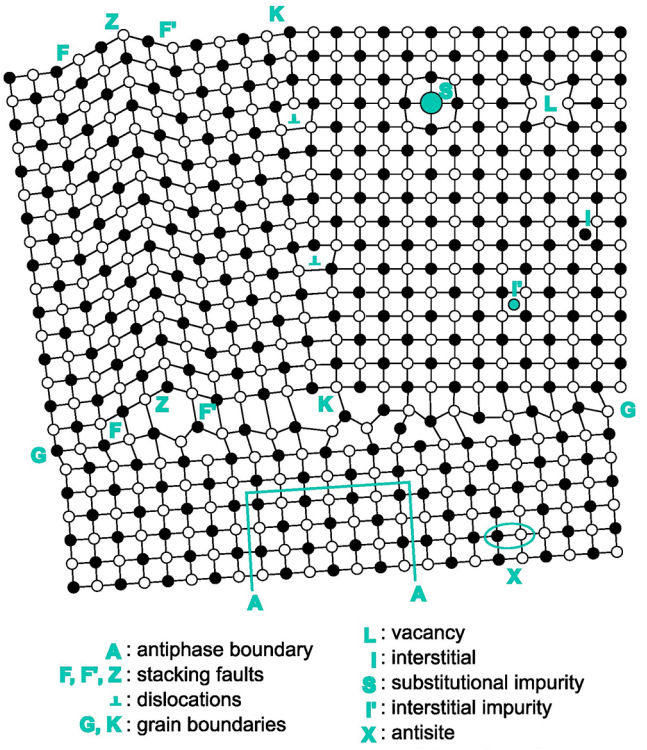

Figure 2. Two-dimensional section of a schematic structure of ordered crystals showing the different types of defects that are often observed in battery materials (redrawn from ref 18).

point defects, which are chemical defects that modify the chemical composition of the compound (see left branch in Figure 1). Among the former ones, *lattice vacancies* (including *Shottky–Wagner defects*; **L** in Figure 2) appear when an atomic site of the ideal crystal is not occupied. At nonzero temperatures, lattice vacancies are always present in any crystal (as they generate disorder in the structure that increases the entropy and stabilizes the system). Vacancies participate in the diffusion mechanism of ionic charge carriers within electrode and electrolyte materials. In higher concentrations (for example, when intercalation-type electrode materials oxidize and mobile alkali cations are removed from the host structure), vacancies can *order* within the crystals (i.e., arrange according to a periodic pattern), which is driven by the minimization of electronic repulsion. The presence of vacancies within the crystal can be detected from a deviation of the intensity of diffraction or solid-state nuclear magnetic resonance (ssNMR) peaks, whereas their ordering with respect to other elements makes appear superstructural peaks in Bragg diffraction and new environments in spectroscopic techniques. *Interstitial defects* (or *Frenkel defects*; **I** in Figure 2) correspond to atoms that have moved from their corresponding atomic site in the ideal crystal to an interstitial position that is normally unoccupied. These defects have a significant impact on the ionic diffusion within electrode and electrolyte materials; in some cases, these interstitial atoms can block the diffusion pathways of mobile ions within the host structure, or if the interstitial defects correspond to mobile ions (i.e., charge carrier), they can be associated with increased conductivity. Likewise, the degradation mechanism of classical alkali (and alkali-rich) TM (transition metal) layered oxides, leading to the formation of spinel-type phases involves the migration of TM and alkali cations into interstitial tetrahedral sites.[15,16] *Antisite defects* (**X** in Figure 2) appear when two atoms exchange their crystallographic sites in the ideal structure. Such defects have been shown to occur between ions with similar ionic radii, such as for example Li^+ and Fe^{2+} ions in a $LiFePO_4$ cathode material, which affects the Li diffusion rate.[17] On the other hand, *extrinsic defects* include *chemical substitutions* of atoms of the original lattice as well as the introduction of an extra atom in an empty *interstitial* site. Note that *aliovalent substitutions* often generate vacancies and/or interstitial defects for charge compensation. These chemical alterations, or *impurities*, (**S** and **I′** in Figure 2) can be introduced accidentally in the material, or intentionally. In this latter case, they are often referred as *dopants* in the case of low concentrations or *chemical substituents* in the case of larger ones. The presence of these foreign atoms within the structure always generates *lattice distortions* and/or *strains* (i.e., a distribution of cell

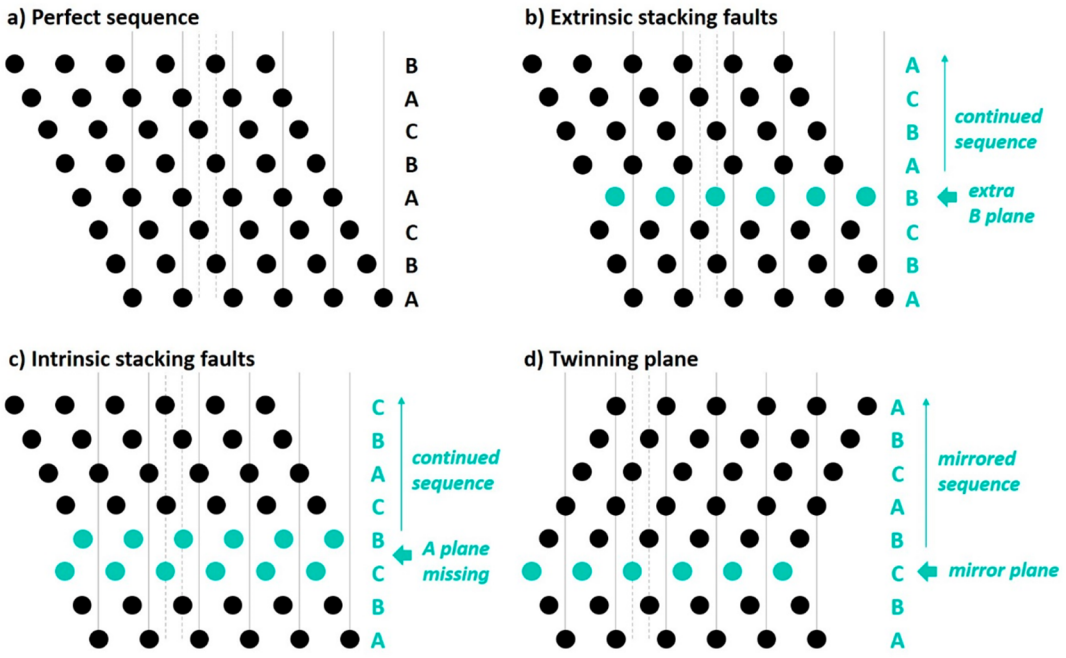

Figure 3. (a) Schematic visualization of an ideal ABCABC stacking sequence. Similar stacking sequences with (b) an extrinsic stacking fault, (c) an intrinsic stacking fault, and (d) twinning of a plane. The layer corresponding to the defect is colored in cyan. Gray lines are guides for the eyes to follow the stacking sequences.

https://doi.org/10.1021/acs.chemmater.2c03481
Chem. Mater. 2023, 35, 3345−3363

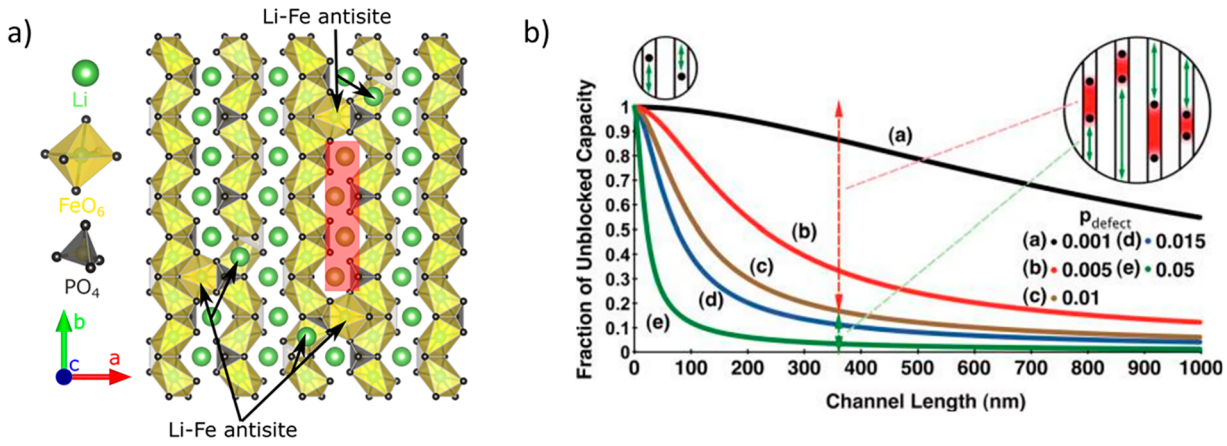

Figure 4. (a) Structure of $LiFePO_4$, where yellow octahedra represent FeO_6, gray tetrahedra represent PO_4, and lithium atoms are represented as green balls. Li−Fe antisite defects block the lithium diffusion channel. If two antisite defects occur in the same channel, some lithium atoms become trapped as those marked with a red square. (b) Computed unblocked capacity vs channel length in $LiFePO_4$ for various defect concentrations. Reprinted with permission from ref 29. Copyright 2010 American Chemical Society.

parameters) because of size and bond modifications. At low concentrations, the extrinsic defects (or *solute*) are generally diluted in the host structure, generating a *solid solution*. A full solid solution can also exist at a larger concentration. However, in some cases, the substituting atom preferentially concentrates in specific regions, forming *clusters*, which can grow until segregating in a *second phase* (*phase separation*). In other cases, the solute is neatly distributed within the host structure, giving rise to an *ordered* configuration (*superstructure*). This ordering can occur at *short* or *long-range*, in turn with more or fewer imperfections, making possible different *degrees of site order/disorder*. Note that here the term *site disorder* refers to a lack of periodicity in the occupation of regular lattice sites within a crystalline structure; it should not be confused with the case of *amorphous* or noncrystalline compounds, where no long-range periodicity exists in the atomic arrangement and hence the atoms cannot be attributed to any lattice site.

Planar defects are bidimensional defects and gather all types of *interfaces*: *intrinsic internal interfaces within the crystal* (detailed below), *free surfaces* (between the crystal and the surrounding gas or liquid), *grain boundaries* (between two crystallites of equal compositions in the particles), and *two-phase interfaces* (between two phases of distinct compositions in the solid, and whose crystal lattice may be coherent, as it occurs in two-phase first-order phase transitions). Free surfaces, grain boundaries (**G** and **K** in Figure 2), and two-phase interfaces result in particular atomic structures that depend on the orientation and have a positive formation energy in comparison to the bulk of the perfect crystal.[13] The nature and properties of these last three types of interfaces have a strong influence on the performance and the processing of battery materials, for example, in the electrode formulation (choice of the additives, formulation recipe and mixing protocol, etc.) or in the processing of solid electrolytes (chemical compatibility, densification approaches, and impact on the ionic conductivity). However, these aspects will not be discussed here; the interested reader is invited to consult other reference papers.[19]

Intrinsic internal defects are planar defects that will be particularly discussed in this perspective paper. They correspond to interfaces (or disruption of the periodicity over a surface) within the crystal. *Antiphase boundaries* (**A** in Figure 2) separate domains of the same ordered phase but with a rupture in the sequence of the atomic distribution. They have been shown to be detrimental to transport and to limit the rate performance of TM-ordered spinel $LiNi_{0.5}Mn_{1.5}O_4$, originating from the formation and propagation mechanism of Ni/Mn ordering in this material.[20] *Stacking faults* mainly appear in layered materials (**F**, **F′**, and **Z** in Figures 2 and 3), although strictly speaking they can be observed in any structure as long as it can be described with a stack of atomic slabs. They correspond to a defect in the sequence of planes of atoms in the crystal and can also be viewed as gliding (or a shift of a whole plane of atoms) with respect to their expected position in the ideal stacking. Stacking faults are divided into three groups (see Figure 3): *extrinsic stacking faults* (insertion of an extra plane in the perfect sequence ...ABC|B|ABC...), which can be the result of many interstitials that gather on planes; *intrinsic stacking faults* (removal of a plane from the perfect sequence ...ABC||BCABC...), which can be the result of the condensation of vacancies on a plane or the slip of the crystal caused by the motion of a dislocation; and *twin boundaries* (plane separating two mirror sequences in the crystal ...ABCAB|C|BACBA...), which are usually introduced during the growth of the crystal.[13] Stacking faults can arise during crystal growth (i.e., they require bond breaking and the creation of new bonds) or from a plastic deformation (i.e., no bond breaking) and are surrounded by dislocations in the atomic structure. They occur in a variety of battery materials, as discussed later in this Perspective. They have been observed either isolated, randomly distributed within the crystals, or condensed, resulting in successive stacking faults in certain regions of the crystal. When the number of stacking faults increases, it may become difficult to identify what would be the ideal stacking sequence, as it occurs in certain lithium-rich layered metal oxides,[21,22] and the structure is then described as a *random stacking*.[14] It should, however, be noted that in such case only the stacking sequence is random, while there is a limited number of possible relative positions (stacking vectors) between the successive slabs. If the layers are stacked out of alignment, the structure is *turbostratic*. Finally, *polytypic* materials are compounds that can occur in different structures, which differ in their stacking sequences. One of the simplest examples is graphite, which crystallizes as hexagonal 2H (stacking sequence ABAB) but often exhibits extended regions of the rhombohedral 3R polytype (stacking sequence ABCABC). In the case of ZnS, CdS, or SiC, polytypic sequences are made of blocks of hundreds of layers. Polytypic structures are prone to exhibit *stacking faults*, but also to lead to *intergrowths* of the different polytypic stackings (like graphite). Note, however, that the concept of structural *intergrowth* is not limited to polytypic structures but could also occur with compounds with similar structure, as has been proposed in Li-rich materials, which would consist of nanometric Li_2MO_3 and $LiMO_2$ intergrowths (both layered structures with the same oxygen lattice)[23,24] or with polymorphs of the same composition (e.g., the cathodic material of alkaline batteries γ-MnO_2 is described as a 3D intergrowth of pyrolusite and ramsdellite domains).[25,26] Selected examples of intrinsic and planar defects in battery materials and their impact on their electrochemical properties are described below in more detail.

https://doi.org/10.1021/acs.chemmater.2c03481
Chem. Mater. 2023, 35, 3345−3363

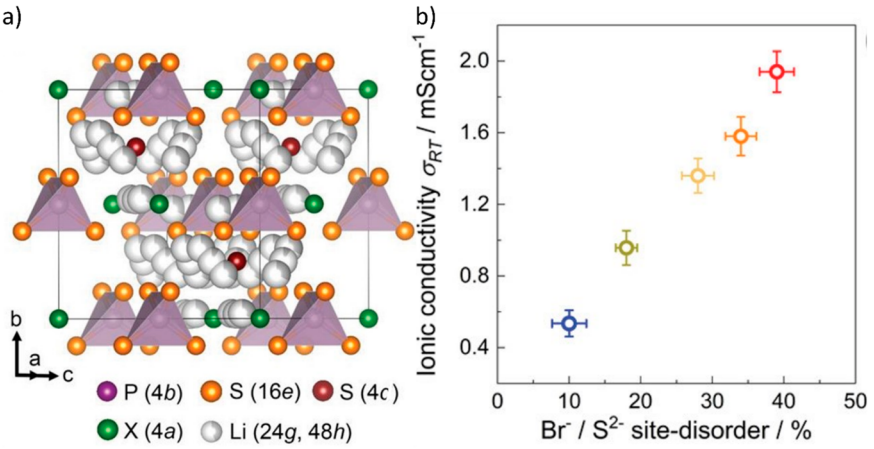

Figure 5. (a) Crystal structure of Li_6PS_5Br shown in an anion-ordered state with Br^- located on the Wyckoff 4*a* site and S^{2-} on the Wyckoff 4*c* and 16*e* sites. (b) Room-temperature ionic conductivity plotted versus the degree of Br^-/S^{2-} disorder. Reproduced from ref 38 under the CC BY-NC 4.0 license.

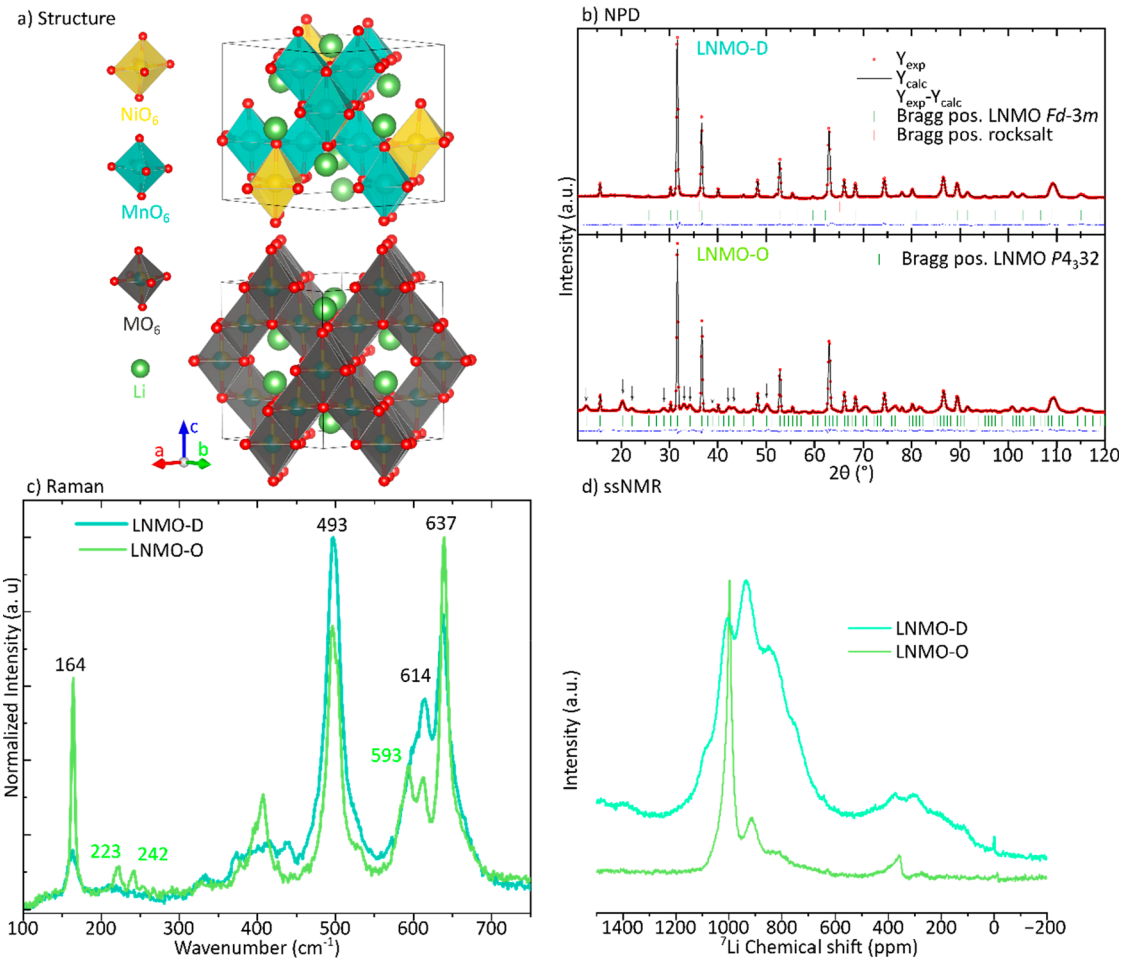

Figure 6. (a) Structure of ordered (top) and disordered (bottom) LNMO. Color coding is as follows: in yellow, NiO_6 octahedra; in cyan, MnO_6 octahedra; in gray, MO_6 octahedra (being M = 1/4Ni and 3/4Mn); and in green, Li atoms. (b) Raman spectra, (c) NPD patterns, and (d) ssNMR spectra of ordered (LNMO-O) and disordered (LNMO-D) samples. Adapted with permission from ref 39. Copyright 2022 American Chemical Society.

INTRINSIC DEFECTS IN BATTERY MATERIALS

Antisite Defects, Site Disorder, and Antiphase Boundaries. *Triphylite LiFePO$_4$.* $LiFePO_4$ (170 mAh/g of theoretical capacity at 3.45 V vs Li^+/Li) is increasingly used in commercial Li-ion batteries as a positive electrode material. Its *triphylite*-type structure (space group (SG) *Pnma*) is based on a solid polyanionic framework made of FeO_6 octahedra and PO_4 tetrahedra, which confer thermal and structural stability to

https://doi.org/10.1021/acs.chemmater.2c03481
Chem. Mater. 2023, 35, 3345−3363

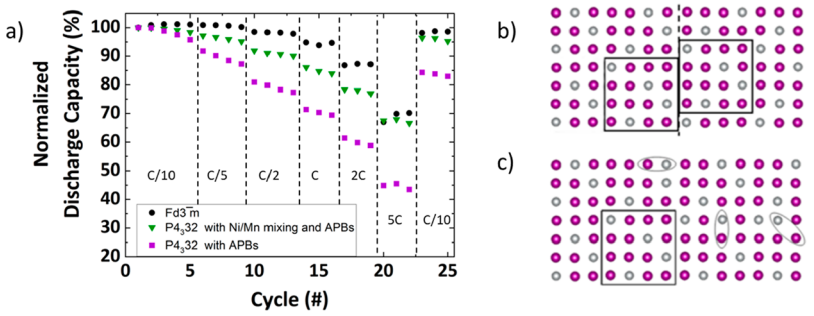

Figure 7. (a) Discharge rate capability test for spinel samples crystallizing in $Fd\bar{3}m$ SG (disordered), $P4_332$ SG with Ni/Mn mixing and antiphase boundaries, and $P4_332$ SG with antiphase boundaries. (b) Antiphase boundaries in an ordered $P4_332$ spinel. (c) Ni and Mn mixing in an ordered $P4_332$ spinel. In both cases, gray and pink atoms represent Ni and Mn atoms, respectively. Oxygen and lithium atoms are not shown for simplicity. Adapted from ref 20 with permission from the Royal Society of Chemistry.

the material, e.g., upon long electrochemical cycling (Li extraction/insertion). Li cations occupy octahedral sites in the straight channels arising from the arrangement of FeO_6 and PO_4 polyhedra. Because of the similar ionic radii between Li^+ and Fe^{2+} (0.76 and 0.78 Å,[27] respectively), *antisite defects* (Figure 4) are widespread in $LiFePO_4$, as demonstrated both experimentally and theoretically.[17,28] In relevant concentrations, these can be detected with ssNMR and X-ray diffraction (XRD) or neutron powder diffraction (NPD). However, in the case of $LiFePO_4$ materials synthesized under optimal conditions (and therefore with low antisite defect concentrations (~1%)), they can be indirectly probed using ssNMR by measuring the diffusion exchange rate between Li atoms in the solid enriched with ^6Li and the liquid electrolyte solution (containing natural abundance Li, namely, 7.6% ^6Li and 92.4% ^7Li).[17] Since $LiFePO_4$ exhibits one-dimensional transport paths, these point defects have a twofold impact: (i) Fe atoms residing in the Li^+ conduction path obstruct Li^+ diffusion, blocking a fraction of the channel if two or more defects occur in the same tunnel (trapped Li atoms, marked with a red area in Figure 4a), and (ii) Li^+ crossover between channels occurs, albeit at a slower rate than Li^+ hopping within the channels.[29] The net effect is typically a reduction in the Li^+ diffusion rate (see Figure 4 b). Small and homogeneous dimensions along the diffusion axis should be used to avoid the negative effects of these defects in the electrochemical performance of $LiFePO_4$.

Halogenated Argyrodite Li_6PS_5X (X = Halogen). The high ionic conductivity offered by Li_6PS_5X (X = Cl, Br) compounds (10^{-4}–10^{-2} S/cm) has triggered great interest for this family of Li^+ ion conductors.[30,31] The ideal, ordered structure of these argyrodite-type Li_6PS_5X (X = Cl, Br, I) compounds is described in a $F\bar{4}3m$ cubic unit cell, as shown in Figure 5a. It is built on PS_4 tetrahedra and a sublattice of isolated halide and sulfide anions, which respectively occupy the 4*a* and 4*c* Wyckoff sites of the $F\bar{4}3m$ unit cell in the ordered configuration, while Li^+ cations are clustered in cages around the 4*c* site. Depending on the halogen, a different degree of anionic disorder has been reported between the 4*a* and 4*c* sites (from a small amount of antisite defect for X = I up to 60% of site disorder for X = Cl).

The lithium conductivity of these compounds has been found to mostly depend on the degree of disorder in the occupancies of anionic and cationic sites. Computational studies have shown that the nature of the halogen does not implicitly govern the ionic conductivity for a given degree of disorder, but the distribution of the halogen in the anionic sublattice affects the Li^+ distribution and conduction pathways.[32−38] The degree of anionic disorder for a given composition was shown to depend on the synthesis parameters, thus enabling the control of the ionic conductivity of the electrolyte material (Figure 5 b).[38] The substitution of P by Ge was also found to induce anionic disorder in $Li_{6+x}P_{1-x}Ge_xS_5X$, improving the ionic conductivity.[32,34] As with other electrolyte materials, the ionic conductivity of the functional component is also affected by the processing of the material; however, this aspect is out of the scope of this Perspective.

Spinel $LiNi_{1/2}Mn_{3/2}O_4$. $LiNi_{1/2}Mn_{3/2}O_4$, which has recently been attracting a large amount of interest as a high-voltage cathode material for the next generation of Li-ion batteries (147 mAh/g of theoretical capacity at ~4.7 V vs Li^+/Li), can crystallize in two polymorphs depending on the ordering of Ni and Mn in the octahedral sites of the spinel structure as shown in Figure 6 a: $P4_332$ (TM *ordered phase*) and $Fd\bar{3}m$ (TM *disordered phase*), with a reversible transition between them observed at ~700 °C. Above the transition temperature, manganese thermal reduction results in the formation of Mn^{3+} defects (resulting in electronic conductivity gains), which is compensated (or driven) by the segregation of a secondary oxide that crystallizes in a rock salt structure and has an increased Ni/Mn ratio, whose insulating nature is detrimental to electrochemistry. Since this secondary phase forms through the preferential extrusion of Ni out of the spinel particles, the amount of the rock salt phase is correlated with the amount of Mn overstoichiometry in the spinel. Added to this, two different types of defects with significantly different effects on properties can be found in ordered samples: (i) antiphase boundaries, which consist of relative displacements of the ordered superlattice that result in a selective broadening of superstructure reflections in NPD data (marked with gray arrows in Figure 6 c) and lead to poor rate performance, and (ii) Ni/Mn mixing (i.e., a certain degree of disorder within the ordered phase), which can lead to an electrochemical performance competitive with that of fully disordered samples (see Figure 7).[20] Both types of defects, even if occurring simultaneously, can only be reliably quantified from NPD data.[20,39] However, spectroscopic techniques such as Raman spectroscopy can be used for facile and reliable discrimination between ordered and disordered forms thanks to their sensitivity to local symmetry (Figure 6 c). Likewise, while the Li ssNMR spectrum of the ordered phase is dominated by a sharp peak as a result of a single lithium environment, the disordered one presents a wider distribution of different Li

https://doi.org/10.1021/acs.chemmater.2c03481
Chem. Mater. 2023, 35, 3345−3363

environments, resulting in multiple peaks (Figure 6 d).[39,40] Achieving control of all these parameters (Mn^{3+} defects and overstoichiometry, Ni/Mn disorder, and the rock salt phase) through the synthesis conditions (synthesis temperature and oxygen partial pressure) is essential to design $LiNi_{0.5}Mn_{1.5}O_4$ electrodes that are closer to the performance limit that the material can offer.[41]

Stacking Faults in Layered Materials. *Layered Oxides.* Lithium layered oxides with the general formula $LiMO_2$ (where M is one or more metals, mainly 3d TMs such as Co, Ni, and/or Mn) are the most used commercial Li-ion cathode materials. Their ideal structure can be described as an ordered α-$NaFeO_2$-type rock-salt in which Li^+ and TM cations occupy alternate layers of octahedral sites of the *fcc* array of oxygen atoms (ABCABC oxygen stacking sequence; Figure 8 a). This regular stacking of LiO_2 and MO_2 slabs corresponds to an *O*3 sequence according to Delmas' notation, in reference to the coordination of the alkali cation in the LiO_2 interslab (T stands for tetrahedral, O stands for octahedral, and P stands for prismatic) and to the number of repeated MO_2 slabs required to describe the periodicity of the unit cell.[42] When the TM layers include different 3d metals, these are usually considered to be randomly distributed in the 3*b* Wyckoff sites in the $R\bar{3}m$ SG, as no sign of superstructure ordering is detected at long-range from XRD or NPD techniques. However, in some specific cases, local ordering trends have been detected using ssNMR, pair distribution function (PDF), or SAED, even if these are lost in the long-range.[43,44]

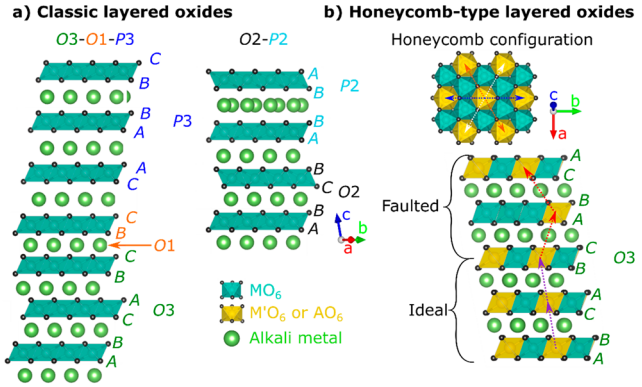

Figure 8. (a) Different possible stacking sequences in classic layered oxides comprised in one schematic structure, with Delmas notation.[42] Cyan octahedra represent TM oxide octahedra, and green spheres represent alkali metals. (b) On top, the honeycomb configuration typical for the alkali-rich layered oxides is shown, where the yellow octahedra represent alkali or alternative metal oxide octahedra. On the bottom, an example of a structure with ideal and faulted stacking is shown. Dashed arrows mark the relative position of the TM slabs.

Upon oxidation, $LiMO_2$ materials often undergo several phase transformations from the ideal *O*3 structure to distorted *O*3′ structures (associated with a symmetry lowering from $R\bar{3}m$ to monoclinic *C*2/*m* due to lithium/vacancy ordering and/or collective Jahn−Teller (JT) distortions) and even to *O*1 (ABAB oxygen stacking; see Figure 8 a) at high delithiated states. In some cases (e.g., $LiCoO_2$), one (or more) hybrid *H*1−3 phases consisting of alternating *O*1 and *O*3 blocks are observed before the appearance of the *O*1 phase. The mechanism of these phase transformations between *O*3, *O*′3, *O*1, and *H*1−3 structures involves slab gliding and often results in interlayer space reduction and the appearance of stacking faults.[6,45] In the case of $LiNiO_2$, the hybrid *H*1−3 phase is not observed upon Li removal/uptake, but *O*1-type defects appear in the *O*3 framework as soon as all the Li atoms are removed from an interslab. In addition, $LiNiO_2$ materials often exhibit off-stoichiometry (Li/Ni ratio <1), which comes along with the presence of Ni^{2+} cations in the Li interslabs. While the presence of Ni in the Li interslabs is presented as detrimental for the electrochemical performance (e.g., further contraction of the interlayer spacing upon oxidation, lower Li diffusion), the fact that *O*3-type defects corresponding to Ni-containing interslabs have been observed in the oxidized O1 structure (see Figure 8 a) suggests that these defects could also have a beneficial effect by preventing the slab gliding to the *O*1 staking sequence.[46] In mixed compositions, the presence of Co in $LiNi_{1-y-z}Co_yAl_zO_2$ (NCA) and $LiNi_{1-y-z}Mn_yCo_zO_2$ (NMC) reduces the degree of Li/Ni off-stoichiometry, although some Li/Ni antisite mixing is still observed. Like in the pure $Li_{1-x}Ni_{1+x}O_2$ materials, the amount of these defects is highly dependent on the synthesis conditions and should be carefully characterized for each sample to well understand their impact on the electrochemical performance. To do so, it is common practice to evaluate the relative intensities of (003)/(104) reflections in the XRD patterns,[47,48] but these can only be decoupled from anisotropic size broadening if a full pattern analysis is performed. In both NCA and NMC, the random distribution of the metals prevents Li/vacancies ordering upon cycling, suppressing most abrupt phase transitions, including the absence of transformation toward the *O*1 phase in the case of NCA. Besides, in partially deintercalated Li_xMO_2 (typically around $x \sim 0.5$ or lower), the TM tends to gradually migrate from the TM slabs to the Li interslabs (i.e., interstitial and antisite defects), which progressively results in the more stable spinel $Li_xM_2O_4$ and/or cation-disordered rocksalt $Li_xM_{1-y}O_4$ phases. This kind of transformations has a strong driving force, but its kinetics can be slowed with an optimal TM-substituted composition.[6,49]

Sodium layered oxides are sought as a cheaper and more sustainable alternative to their lithium homologues. Depending on the chemical composition and synthesis conditions, they crystallize into a wider variety of stacking sequences in addition to *O*3,[50,51] such as *P*3 (ABBCCA oxygen stacking sequence)[52] or *P*2 (ABBA oxygen stacking sequence).[50,53−58] In the *P* stacking sequences, the alkali metal lays in prismatic positions, for which the space between adjacent sodium atoms is smaller. Na−Na repulsions strongly destabilize the structure and therefore only sodium-deficient *P*-type materials can be obtained (generally $Na_{2/3}MO_2$). It should be noted that the five types of "primary" stacking sequences (illustrated in Figure 8 a) and their derivatives (distortions or polytypic intergrowths of these "primary" stacking sequences) can be separated into two groups: on the one hand *O*3, *P*3, and *O*1, and on the other hand *P*2 and *O*2. Phase transitions between phases of a same group can occur by simple layer gliding, while the phase transformations between two groups require M−O bond breaking and are therefore thermodynamically unfavored. In other words, transitions between *O*3, *P*3, and *O*1 phases and between *P*2 and *O*2 ones can occur during electrochemical cycling, while transitions between the two types are forbidden. However, although slab shearing does not require bond breaking and can be seen as easily reversible, in certain cases where the phase transformations involve important structural changes (e.g., contraction/expansion of the interslab distances)

https://doi.org/10.1021/acs.chemmater.2c03481
Chem. Mater. 2023, 35, 3345−3363

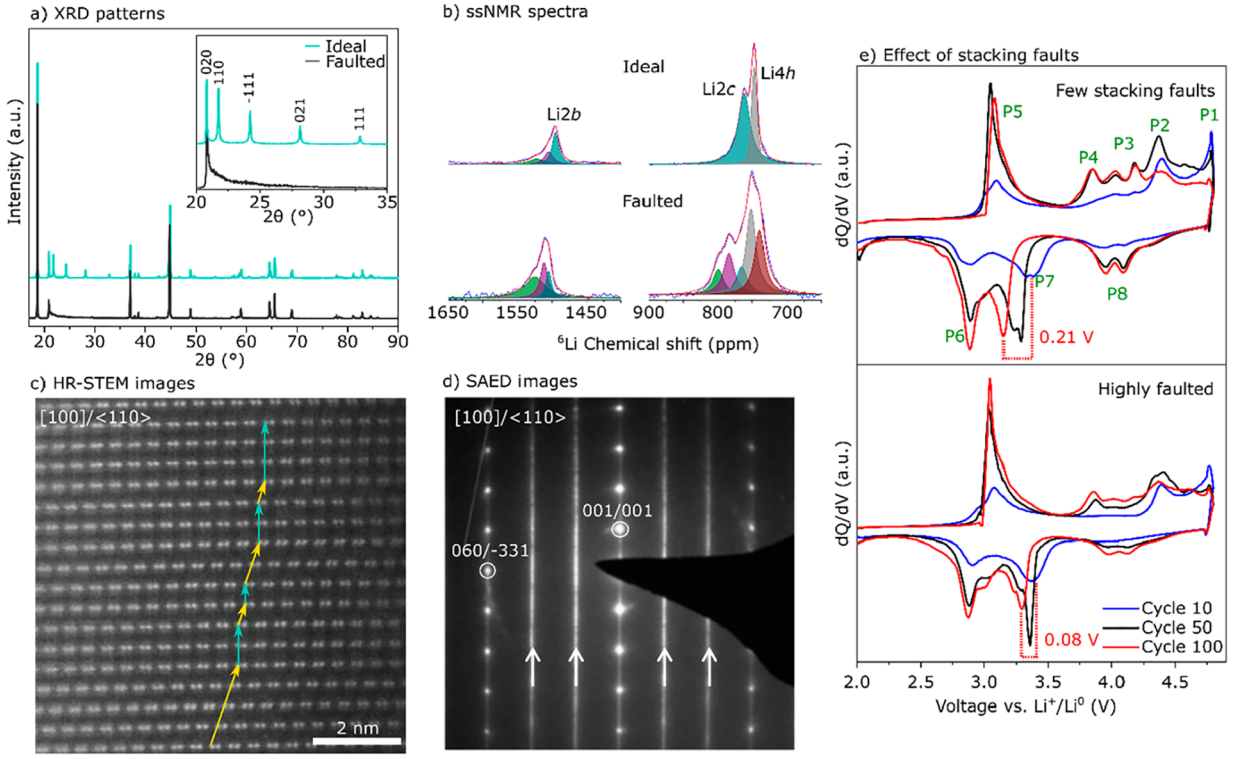

Figure 9. (a) Experimental XRD patterns of an ideal (in cyan) and a defective (in gray) Li_2MnO_3 sample. While the ideal sample shows five well-defined peaks in the $2\theta_{Cu}$ range 20−35° related to the ordering in the TM layer, the highly faulted sample shows an asymmetric peak. (b) Deconvoluted ^{6}Li MAS ssNMR spectra of the ideal and defective samples from panel a. The defective sample shows a larger number of peaks due to the new local environments generated by the stacking faults. Adapted with permission from ref 92. Copyright 2019 American Chemical Society. (c) HR-STEM images of defective Li_2MnO_3. The bright points correspond to manganese columns. The faulted stacking can be followed with the cyan and yellow arrows. (d) SAED pattern of the defective sample shown in panel c. Diffuse lines marked with white arrows evidence the existence of a significant amount of stacking faults in the material along the *c*-axis. (e) d*Q*/d*V* plots for Li_2MnO_3 samples with low and high degrees of stacking faults, showing how the characteristic voltage fading of these compounds is retarded in the sample with more defects. Adapted from ref 21 with permission from the PCCP Owner Societies.

it can lead to structural damage after extended cycling. For this reason, some research efforts have been focused on avoiding abrupt phase transformations, as it will be illustrated below.

*O*3-Type $NaMO_2$ materials (e.g., M = Co, Ni, Cr) typically transform into layered *P*3-type phases at the beginning of Na^+ deintercalation, while $NaVO_2$ materials maintain a distorted *O′*3-type stacking until half the Na ions have been removed.[6,49,59,60] Vacancies and Na atoms tend to order in both *O*3- and *P*3-type structures upon Na deintercalation to maximize the distance between alkali cations, which is reflected though multiple voltage steps in the galvanostatic curves. Complex Na/vacancies ordering schemes are observed in the *P*3-type structures, giving rise to Na-rich and Na-poor ordered domains that are separated by antiphase boundaries and enable the accommodation of changes in the Na composition.[10] The presence of these antiphase boundaries might also have implications in the Na diffusion mechanism, either through the facile 1D diffusion of Na^+ along Na-poor antiphase boundaries or through the displacement of antiphase boundary waves throughout the crystal.[10] Selected TM substitutions have been suggested to prevent or delay the transition from *O*3 to *P*3, which could thus reduce mechanical degradation due to repetitive phase transformations.[61] Contrary to Li-based layered oxides, TM migration to the NaO_2 interslabs was calculated to be unfavorable for both *O*3- and *P*3-type half-desodiated structures due to the larger size of Na^+.[49] Migration of Fe in *O*3-type $NaFeO_2$ is, however, experimentally observed at high desodiation states.[62]

*P*2-Type materials such as $Na_{2/3}[Ni_{1/3}Mn_{2/3}]O_2$ transform into *O*2-type phases through a biphasic reaction upon desodiation. In contrast, *P*2-$Na_{2/3}[Fe_{1/2}Mn_{1/2}]O_2$ has been reported to undergo a more complex desodiation mechanism, where Na removal is compensated by the progressive introduction of vacant *O*-type stacking faults into the *P*2 structure. This gives rise to a continuously changing intergrowth of *P*2 and *O*2 blocks (sometimes referred to as "*Z*"-phase), which evolves toward the final *O*2-phase through an ordered *OP*4-type intermediate that is made of a perfect alternation of *P*2 and *O*2 slabs.[63]

Alkali-Rich Layered Oxides. Lithium-rich (Li-rich) layered oxides with the general $Li[Li_xM_y]O_2$ formula (where M is typically Mn, Ni, and/or Co; $x + y = 1$; and $0 < x \leq 1/3$) can be regarded as conventional *O*3-type layered oxides in which TMs are partially replaced by lithium.[64] Some groups describe the structure as an intergrowth of Li_2MnO_3 and $LiMO_2$ domains,[24,65−70] while others describe them as a full $Li_{1+x}M_yO_2$ solid solution;[22,71−74] and the only reconciling explanation found so far is that differences in the synthetic method may lead to one or the other.[75] These materials can deliver high capacities of over 250 mAh/g at similar voltages as conventional layered oxides, leading to energy densities above 1000 W·h/kg. This high capacity arises from the combination of cationic and anionic redox activity.[64,76−78]

https://doi.org/10.1021/acs.chemmater.2c03481
Chem. Mater. 2023, 35, 3345−3363

However, anionic redox activity often comes together with structural irreversible modifications, which result in a low initial Coulombic efficiency (ICE) and continuous voltage and capacity decay.[64,79−82] Proper understanding of the structure of these materials is vital to overcome capacity and voltage fading. Owing to size differences between the Li and TM atoms, these tend to order following a honeycomb-like configuration (i.e., each Li is surrounded by 6 TMs in the Li_2MO_3 composition, as shown in Figure 8 b). While keeping the *O*3-type stacking sequence unchanged (ABCABC oxygen stacking), the stacking of these ordered layers can follow three different directions, as shown in Figure 8 b with white, orange, and blue dashed arrows over the honeycomb-like view. The continuous stacking along the same direction results in an ordered structure (e.g., purple dashed arrows in Figure 8 b). Yet, stacking faults involving all three stacking directions are often encountered in these materials depending on the synthesis conditions (red dashed arrows in Figure 8 b), with examples that often show negligible long-range order in the stacking direction.[21,83−85]

The cationic ordering within the TM slabs of the Li-rich layered structures results in new characteristic features in XRD, NPD and selected area electron diffraction (SAED) patterns (i.e., superstructure reflections), ss-NMR spectra (i.e., additional Li environments), or HR-STEM images (i.e., dumbbell column of TM atoms separated by invisible columns of Li), which are in turn distinctively altered by the presence of stacking faults. Examples for each of these techniques, corresponding to an ordered and a highly faulted Li_2MnO_3 sample, are shown in Figure 9. Figure 9 a compares the experimental XRD patterns of the two materials. The XRD pattern of the ordered sample shows well-defined superstructure peaks (020, 110, −111, 021, and 111) arising from the honeycomb ordering. When stacking faults are present, these peaks are anisotropically broadened and, at larger concentrations, they merge into one asymmetric broad peak sometimes referred as a *Warren fall*.[21,84,86−88] Figure 9 b shows the corresponding ^{6}Li MAS ssNMR spectra of the same two materials. While the ordered structure exhibits mainly three peaks related to the three different Li environments, the spectrum of the faulted structure shows extra peaks due to the presence of new local environments, which was confirmed by DFT calculations.[89−94] Alternatively, stacking faults can be directly observed by high-angle annular dark field scanning transmission electron microscope (HAADF-STEM) images (Figure 9 c) due to the *Z* contrast difference between the TMs and the lithium.[21,70,88,95,96] Additionally, the SAED patterns exhibit continuous diffuse scattering lines along the stacking direction instead of well-defined diffraction spots (Figure 9 d).

Although stacking faults can be easily identified, they are often omitted from the structural characterization because their modeling and quantification has been traditionally challenging. However, stacking faults are commonly present in large amounts, and their effect on the electrochemical performance should not be ignored. Classic XRD and NPD refinement methods such as Rietveld (least squares approach to refine a calculated powder diffracton profile until it matches the measured profile) enable the extraction of information from ideal structures and structures with particular defects, such as point defects or antiphase boundaries. However, they fail to model the complex anisotropic broadening caused by structures containing planar defects. Alternatively, computer programs such as TOPAS,[97] or FAULTS[25,98] (which in turn is based on DiFFaX[99]), allow such defect structures to be described by using averaged supercells or stacks of structurally different atomic layers, respectively. With this approach, SAED images of specific planes can also be simulated by FAULTS; and XRD and NPD patterns of structures presenting planar defects such as stacking faults can be simulated and refined.

The role of stacking faults in the electrochemical performance of Li-rich layered oxides has been investigated by several authors.[21,64,83,100] As occurs with many defect structures, the main difficulty consists in decoupling the impact of stacking faults from that of the size of crystallites or particle morphology. Indeed, the synthetic conditions favoring stacking faults generally result in smaller crystallites. A systematic study comparing samples with different microstructural characteristics concluded that samples with stacking faults exhibit less voltage fading. The characteristic voltage fading of this material is primarily seen in the displacement of the discharge peak at 3.3 V (which charges at 4.3 V) to lower voltages. This is shown in Figure 9 e, where the dQ/dV plots for two Li_2MnO_3 samples with similar particle sizes and different degrees of stacking faults are compared.[21] This degradation was theoretically studied in ref 101.

Research in Na-rich batteries is becoming of increasing interest, as they crystallize with the same structure as the Li-rich homologues. However, their behavior upon cycling is more complex.[102−106] The model compound *O*3-Na_2RuO_3, which exhibits a large amount of stacking faults in the pristine state, shows a reversible and spontaneous ordering upon charging, which was explained as a cooperative effect to maximize the alkali-vacancy Coulombic attraction and minimize the alkali-TM cationic Coulombic repulsion.[102]

In addition to lithium- and sodium-rich layered oxides, other battery materials exhibit honeycomb ordering of the cations. Examples are the $LiTiO_2$−Li_2TiS_3 system,[107] or $A_2M_2TeO_6$ (A = Na, K, Ag; M = Ni, Co, Zn, Mg) tellurates.[106,108−113] These later materials exhibit *P*2 structures. However, the honeycomb-type slabs can stack following a single stacking direction like in K_2NiTeO_6[113] (straight configuration, SG $P6_3/mcm$, Figure 10

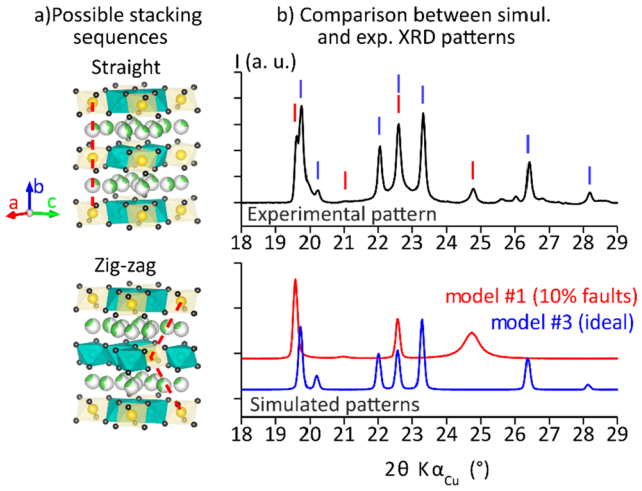

Figure 10. (a) Visualization of straight and zigzag-type stacking sequences. Red dashed lines are a visual guide to help to follow the stacking. (b) Comparison between the experimental pattern in black (top) and two simulated models in red and blue (bottom). Adapted with permission from ref 111. Copyright 2021 American Chemical Society.

https://doi.org/10.1021/acs.chemmater.2c03481
Chem. Mater. 2023, 35, 3345−3363

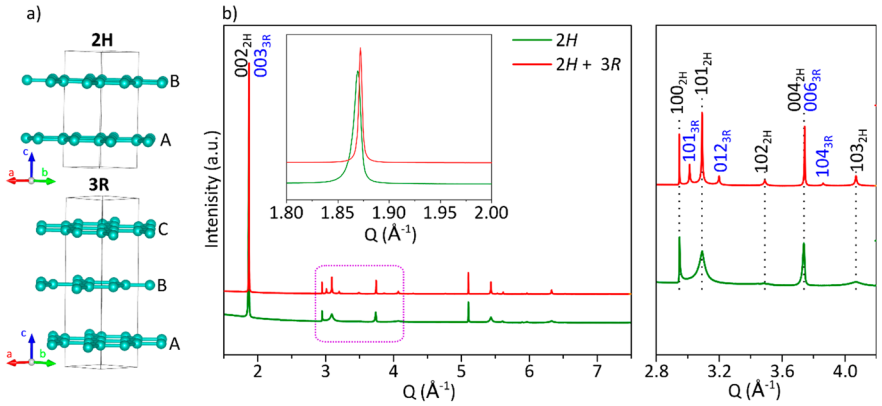

Figure 11. (a) Structures of 2*H* and 3*R* graphite polytypes. Cyan spheres represent the carbon atoms. (b) Experimental XRD patterns of two different graphites: a 2*H* phase containing stacking faults and turbostratic defects, as revealed by the anisotropic broadening of the some of the 2*H* reflections (green pattern), and an intergrowth of 2*H* and 3*R* phases (red pattern) showing a lower number of stacking faults and turbostratic layers. The reflections corresponding to the 2*H* phase are indicated with dashed lines as guides for the eyes for both patterns.

a) or alternate between two stacking directions like that in Na_2NiTeO_6 (zigzag configuration, SG $P6_322$, Figure 10 b).[111,112] Interestingly, mixed Na and K compounds exhibit ordered pure K and pure Na layers, resulting in an additional superstructure in the stacking direction in which K and Na layers alternate.[111−113] This material exhibits stacking disorder and, according to FAULTS simulations, the structure can be described as a combination of straight stacking of the potassium layers with a combination of straight and zigzag sequences for the sodium ones,[111] which was in accordance with independent HR-STEM images.[112]

Nickel Hydroxides. Brucite-type β-$Ni(OH)_2$ is used as cathode material in NiCd and NiMH batteries. Its structure, described in a hexagonal unit cell (SG $P\bar{3}m1$), is based on an ABAB oxygen stacking sequence that results in edge-sharing NiO_6 octahedral layers, with protons filling the interlayer tetrahedral sites ($T1$-type structure). When oxidized to β-NiOOH, the material undergoes a reversible change in the oxygen stacking sequence, resulting in a metastable $TP2$ stacking.[114,115] Commercial electroactive forms of β-$Ni(OH)_2$ have long been considered to be "badly crystallized" or of "low crystallinity" because of the strong broadening of certain reflections in the powder diffraction pattern, although the precise description of such broad concept was poorly understood.[116] However, the implementation of advanced microstructural models in Rietveld refinement analysis accounting for anisotropic size broadening revealed that such "bad crystallinity" consisted mostly of short coherence lengths resulting from the small size of the crystallites along certain directions (a few nm).[117] Stacking faults, also previously proposed as the main cause of anisotropic peak broadening,[118−120] have also been observed in HRTEM images of β-$Ni(OH)_2$;[121] however, their quantification remains elusive due to the coupled preponderant effect of size broadening in the diffraction pattern.[117,121] All in all, the thorough understanding of the microstructures of different series of β-$Ni(OH)_2$ samples established that both the crystallite size and the presence of stacking faults have a synergic effect on the improvement of sample performance.[121]

Graphite. Graphite is the negative electrode of choice in commercial Li-ion batteries due to its excellent performance (372 mAh/g of theoretical capacity at 0.25−0−01 V vs Li^+/Li) and relatively low price.[122] Graphite crystallizes as a stacking of graphene layers linked through van der Waals weak interactions in a hexagonal 2*H* (ABAB, $P6_3/mmc$) stacking sequence (Figure 11 a). However, it often contains stacking faults and/or extended domains of rhombohedral 3*R*-like polytype (ABCABC, $R\bar{3}m$, see Figure 11 a) and turbostratic layers.[122−127] All these defects have an impact on the XRD patterns. Stacking faults can be identified by the selective broadening of certain reflections (i.e., while the 100_{2H} peak is thin, peaks such as 101_{2H} and 103_{2H} are considerably broader), while turbostratic defects broaden the $10L_{2H}$ peaks, where $L = 2n$, and displace the $00L$ peaks to lower angles due to the larger interlayer distance that results of electrostatic repulsions. The presence of the 3*R* phase domains can be easily identified with the appearance of additional peaks (see Figure 11 b). Turbostratic layers have been found to hinder the lithium intercalation reducing the effective capacity,[128] while small amounts of the 3*R* phase were found to improve the thermal stability of the graphite.[129]

Calcium Ferrites. Even if calcium batteries at the very early stages of research, $Ca_4Fe_9O_{17}$ has been proposed, from theoretical calculations, as a possible candidate to be used as a cathode for Ca-ion batteries. It can theoretically deliver 230 mAh/g at 4.16 V with low calculated migration barriers for calcium ions (0.7 eV).[130] Its structure was solved in 1982 from a single crystal and described as alternating layers of FeO_6 octahedra and FeO_5 bipyramids linked by FeO_4 tetrahedra, with calcium ions residing in the empty spaces (Figure 12 a).[131] However, this model fails to fully describe the powder diffraction patterns of samples with the same composition.[130] SAED patterns revealed the presence of stacking faults on the stacking direction, which were described and quantified with FAULTS simulations and refinements of both XRD and NPD patterns (Figure 12 b). The defect structure results from the combination of three possible stacking directions that are randomly stacked (an example of the faulted structure is shown in Figure 12 a). The presence of stacking faults was suggested to be the origin of the bad electrochemical performance despite the low calcium migration barriers, although a systematic study comparing samples with different degree of faulting would be needed to confirm this hypothesis.

Halides. Li_3MX_6 materials, where M = TMs such as Y, Sc, Er, etc. and X = halide, are today at the center of research in superionic conductors, as they have been reported to have

https://doi.org/10.1021/acs.chemmater.2c03481
Chem. Mater. 2023, 35, 3345−3363

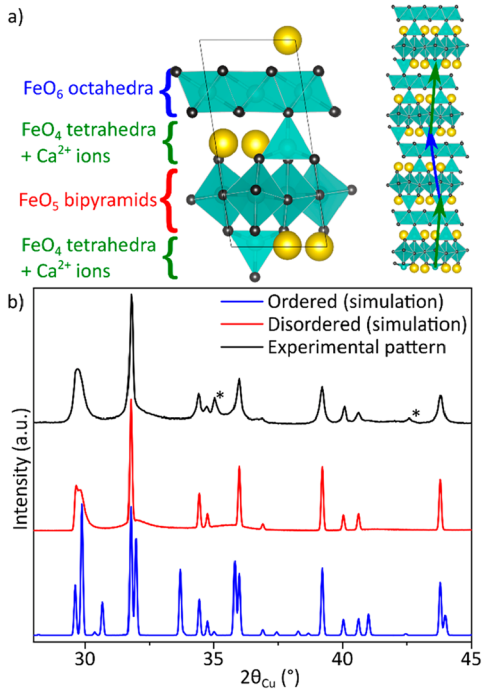

Figure 12. (a) Ideal and faulted structures of $Ca_4Fe_9O_{17}$. (b) Comparison between the experimental XRD pattern (in black) with XRD simulations of an ordered (blue) and a disordered (red) structure. Reproduced from ref 132 with permission from the Chinese Chemical Society (CCS), Peking University (PKU), and the Royal Society of Chemistry.

predicted Li^+ conductivities of around 14 mS/cm and experimental Li^+ conductivities of 0.12 mS/cm[133−141] due to the large number of vacancies and the lower Coulombic interaction between the halide and the lithium atoms in comparison with oxides. They are stable at high voltages and compatible with layered oxides, which makes them particularly attractive. Li_3YCl_6 (LYC) was computed to be the most promising material in terms of activation energy and ionic conductivity.[135] When prepared by ball milling, LYC crystallizes in the $P\bar{3}m1$ SG with Li and Y octahedrally coordinated with the halide atoms, as shown in Figure 13a,b.[142] The broadening or even disappearance of certain XRD peaks related to the planes of the Y atom inhibit a complete Rietveld refinement (Figure 13 c).[140] FAULTS refinement was performed to understand the defect structure, which consists of the combination of Li/Y layers with half Y occupation, lithium-rich layers without Y, and layers with full Y occupation (Figure 13 c). This model was able to successfully describe the broadening of the peaks affected by the stacking faults and was confirmed by cryo-TEM imaging and DFT calculations.[140] Nudged elastic band (NEB) calculations and bond valence (BV) maps confirmed that these faults facilitated ionic conduction. Two different migration paths were calculated in different structural configurations: in the *ab* plane and along the *c*-direction. The results showed a large variation in the migration barriers, but stacking faults generally facilitated the lithium transport because they increased the connectivity between Li sites.

Intergrowths. *EMD-MnO_2.* Electrolytic manganese dioxide (EMD-MnO_2), used a positive electrode material in alkaline primary batteries, represents another insertion compound with planar defects. The electroactive forms of manganese dioxides have been historically classified into γ-MnO_2 and ε-MnO_2 depending on specific features of their XRD patterns, which are typically those of poorly crystalline compounds with few peaks and pronounced anisotropic broadening. The XRD pattern of the latter exhibits some resemblance to the pattern of the ramsdellite mineral (R-MnO_2) while the pattern of the former is closer to that of pyrolusite (β-MnO_2, rutile-type structure).

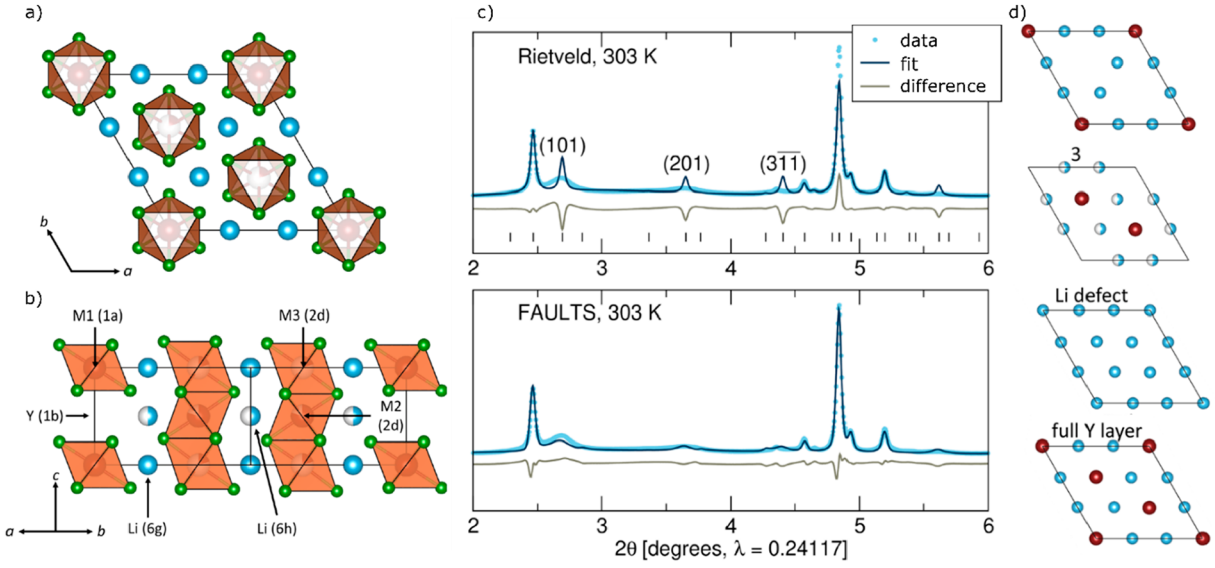

Figure 13. Reported $P\bar{3}m1$ structure of LYC shown from different angles: (a) structure viewed down the *c*-axis and (b) annotated side view of the LYC crystal structure. The structure exhibits full Y occupancy at the M1 (0, 0, 0) position and split Y occupancy over the M2 (1/3, 2/3, 0.5) and M3 (1/3, 2/3, 0) positions. The Wyckoff positions are denoted in parentheses. (c) Comparison between Rietveld and FAULTS analyses of X-ray diffraction data (λ = 0.241 17 Å) of Li_3YCl_6. (d) Individual layers used to build the FAULTS model. Chlorine layers are not shown here for simplification purposes. Orange balls or octahedra represent Y, blue balls represent Li, and green balls represent chlorine. Figure adapted from ref 140 under CC BY-NC-ND license.

https://doi.org/10.1021/acs.chemmater.2c03481
Chem. Mater. 2023, 35, 3345−3363

Both pyrolusite and ramsdellite structures are based on a similar hexagonal close packing (hcp) of oxygen atoms, with half of the octahedral sites occupied by manganese atoms. Mn atoms are arranged in double chains of MnO_6 octahedra in the case of ramsdellite (forming 1 × 2 tunnels for the diffusion of the mobile species; Figure 14 a) and single chains of MnO_6 in the case of pyrolusite (forming 1 × 1 empty tunnels; Figure 14 b).

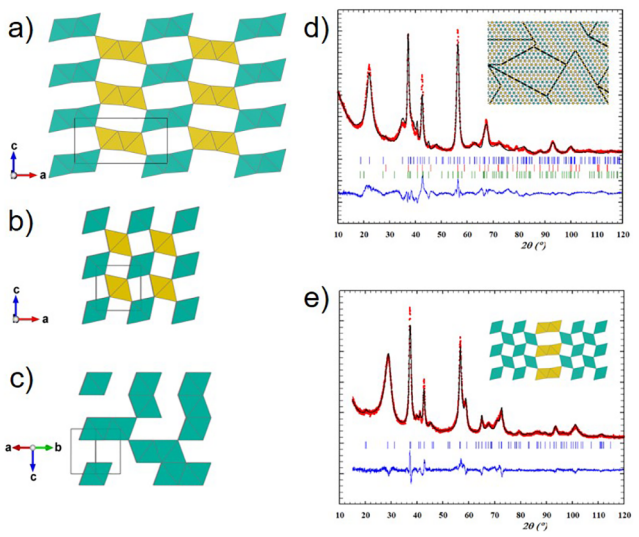

Figure 14. Structural models for the (a) ramsdellite, (b) pyrolusite, and (c) ε-MnO_2 (equivalent to a fully Mn-disordered pyrolusite) phases. (d) Rietveld refinement of EMD-MnO_2 samples using a ramsdellite-type R-MnO_2 phase (Bragg positions indicated with blue sticks), a fully disordered ε-MnO_2 phase (red sticks), and a tiny amount of pyrolusite β-MnO_2 (green sticks). The inset illustrates short-range order crystallites of the R-MnO_2 phase with microtwinning and pyrolusite-type faults (De Wolff defects), which is representative of the ε-MnO_2 disordered superstructure. Redrawn from ref 148. Copyright 1961 AIP Publishing. (e) FAULTS refinement of a γ-MnO_2 sample using a structural intergrowth between pyrolusite and ramsdellite slabs, showing that the sample contains 9% of isolated ramsdellite-type defects in the pyrolusite matrix, as illustrated in the inset. Adapted from ref 25. Copyright 2016 International Union of Crystallography.

The description of the real structure of EMD-MnO_2 samples is thus challenging, and different models have been discussed for the last seven decades. DeWolf and co-workers proposed describing γ-MnO_2 samples as a structural intergrowth between pyrolusite and ramsdellite structures, while the structure of ε-MnO_2 samples was suggested to consist of a statistical (random) distribution of Mn in the hcp array of oxygens (Figure 14 c).[143,144] Later, using the intensity of the two first broad peaks at low angles of the XRD pattern, the γ- or ε-character of the samples was determined (also referred to as the "Q ratio", which is correlated with the increase of the deposition current density, the Brunauer−Emmett−Teller (BET) surface area, the porosity, the pore volume, and the bulk density).[145−147] Then, Chabre and Pannetier proposed describing the wide variety of EMD-samples using the percentages of 1 × 1 tunnels (Pr) and of microtwins (Tw),[26] both pseudoquantitatively determined from the position of selected Bragg peaks that are strongly related to the concentration of these defects, as they demonstrated with series of XRD patterns simulated with the help of the DIFFaX[99] program.

The refinement of XRD data was, however, achieved more recently. On the one hand, XRD patterns whose first peak matches with the main reflection of the ramsdellite structure at low angles can be refined using a Rietveld refinement involving a ramsdellite-type R-MnO_2 phase and a fully disordered ε-MnO_2 phase, with the occasional occurrence of pyrolusite β-MnO_2 (Figure 14 d). Simon and co-workers interpreted that the need for this ε-MnO_2 phase for the refinement does not correspond to a discrete phase, but instead it is the signature of Mn disorder within the long-range ordered oxygen framework, i.e., microtwinning forming boundaries between small domains of ordered ramsdellite-type crystallites (see inset in Figure 14 d).[148] On the other hand, recent advances in refinement software (e.g., FAULTS[25,98] and TOPAS,[97]) enable the refinement of intergrown structures to be performed that was not possible at the time of Chabre and Pannetier's paper. Casas-Cabanas et al. showed that samples with a strong γ-character (i.e., first broad peak indexed with the main peak of the pyrolusite structure) can be refined with a structural intergrowth of pyrolusite and ramsdellite domains using the FAULTS program, making possible a quantitative evaluation of the amount and distribution of ramsdellite motifs into the pyrolusite structure (Figure 14 e).[25] Such structural intergrowth implies the loss of long-range ordering along one direction and prevents conventional Rietveld refinement. Besides, PDF analysis was also evaluated to model and quantify the crystal intergrowth of MnO_2 samples, but it was found to be less suitable than XRD pattern analysis.[149,150]

DISCUSSION AND PERSPECTIVES

Defects Are Ubiquitous in Battery Materials and Their Impacts Remain in Many Cases Poorly Understood. All the examples presented in the previous section illustrate the profound impact of defects on the performance of battery materials. However, accurately describing the nature, location, and amount of defects often represents a challenge due to (i) the limited number of characterization methods able to probe defects and/or their limited application; (ii) the diversity of crystal structures and constituent elements; and (iii) the variety of defects, their nature, and their usually low concentration. Poor understanding of their effects (either beneficial or detrimental) represents a knowledge gap whose negative impact cannot be afforded.

Progress in the Characterization of Defects Is Providing Unprecedented Insights into Defective (and Ordered) Structures. The observation and understanding at the atomic scale have, however, greatly progressed in recent years and are in some cases now ripe for exploitation. Recent models and tools applied to X-ray scattering techniques, often in complement with electron microscopy or ssNMR, offer an accessible window for the observation and accurate parametrization of complex microstructural features. Recent advances in the refinement methods of XRD data have made it possible to move from qualitative or semiquantitative approaches to achieve full pattern fittings and more precise characterization (both qualitatively and quantitatively) of defects. Most Rietveld refinement programs now include approaches to refine structures with antisite defects or antiphase domains, while the FAULTS program[25,98] enables the refinement of systems with any type of planar defects (including those including 3D frameworks). FAULTS refine-

https://doi.org/10.1021/acs.chemmater.2c03481
Chem. Mater. 2023, 35, 3345−3363

ments were also needed to reveal full cationic site ordering in Li_4FeSbO_6, an example that highlights the importance of combined structure and defect descriptions to avoid misleading results.[151]

Need to Invest More Efforts to Develop Techniques and Methods to Study Defects. There are, however, several technical bottlenecks that still require the development of novel methodologies across multiple disciplines. Conventional diffraction, imaging or spectroscopic characterization techniques also suffer from relevant limitations. These either provide indirect information (in powder diffraction, for example, microstructural and structural contributions are convoluted), cover limited length scales, require coherency, are destructive (and therefore low doses might be required with a concomitant loss of sensitivity), are spatially resolved (and therefore nonaveraged), or are limited in contrast for light elements. As a result, attempts to characterize defects are often limited to quasi-ideal materials (which are not always representative) or to "ideally faulted" materials with relatively simple structures. A scenario with several types of defects coexisting represents a major challenge. In diffraction, the angular dependence of the different types of defects is often used to decouple their contribution to line broadening; however, the profile parameters used are often strongly correlated and may lead to an over- or underestimation of the various types of defects. To avoid this, the structural model is often simplified and includes only the defect with the strongest contribution to the diffraction pattern, at the cost, however, of an incomplete description of the defect structure. More efforts should be invested in developing techniques and methods to better characterize defects (and disorder) and correlate their effects in functional materials.

Operando Studies Allow the Dynamic Evolution of Defects to Be Understood. While progress is being made in understanding the role of defects in certain properties, operando studies focusing on defects are still very rare. Such an approach represents an additional degree of complexity, but there is evidence that defects can dynamically evolve and strongly impact on the obtained capacity and the resulting cycle life.[101,102] Breakthroughs in understanding the dynamic evolution of defects are expected to result in unique insights regarding the impact of defects on phase transformations that can be further exploited for the development of a new class of materials through microstructural design.

More Research Is Needed to Cover More Materials and Types of Defects. The diversity of materials, defects, and synthesis approaches requires a collective effort to achieve a complete picture of defects and their dynamic evolution, which is still in its initial steps. One can mention, for example, the fact that stacking faults, despite being observed, have not been extensively studied in ceramic electrolytes such as in halides,[140] oxides,[152] or sulfides,[153] in contrast to those for cathode materials, and further research is needed (and expected) in the coming years to establish correlations with ionic conductivity. Likewise, very few reports dig into the role of interfaces resulting from twin boundaries, antiphase domains, grain boundaries, or intergrowths on lithium transport, although there is recent evidence of a major impact.[154,155]

Another example is the role of dislocations in battery materials. These linear defects are strongly related to stacking faults: stacking faults start and end with dislocations within the particles (it is indeed improbable that materials undergo stacking sequence changes via the macroscopic collective shearing of an entire particle).[10] Dislocation glidings may participate in the phase transformations occurring through slab shearing.[156−158] Achieving a high dislocation energy has thus been suggested as a means to prevent stacking sequence transitions in layered oxides.[10] Operando experiments using Bragg coherent diffractive imaging (BCDI) have recently been proposed to study the contribution of dislocations in the phase transformation mechanism of LNMO and Li-rich layered oxides.[159,160] Finally, several reports also suggest that ionic diffusion can also be amplified or hampered by the presence of dislocations and grain boundaries.[161,162] A new tool has been recently made available to build models of highly distorted local environments representative of dislocations, grain boundaries, and surfaces.[163] All these present new opportunities for improving battery materials through defect engineering.

Systematic Studies of Series of Samples Are Key to Understand the Impact of Defects on the Electrochemical Properties. Understanding the individual impact of overlapping microstructural features on electrochemical properties is a difficult mission. The more reliable approach consists of evaluating samples with a variety of microstructural features and concentrations to establish independent correlations.[121] Such an approach will often require mastering the synthesis conditions that will favor one or the other features, for which a previous screening of different conditions will be required.[21] Although such systematic studies require more time and resources, these are very often the only means to ensure that reliable correlations are established and that synthetic efforts are invested toward the right direction.

Defect Engineering Offers a Unique Design Opportunity to Make Better Battery Materials. While defects have traditionally been thought of as detrimental, we have shown in this review that they can result in novel or improved functionality. As a matter of fact, defects are a sine qua non requisite for lithium transport.[164] However, most microstructural features appear accidentally: as our ability to observe defects is limited, so is our synthetic control. Proper understanding of faulted structures is expected to pave the way toward the directed design of superior materials and to set the ground to the development of novel functionality. Microstructural control offers a unique opportunity to enlarge the chemical design space to foster a new generation of imperfectly perfect functional materials.

AUTHOR INFORMATION

Corresponding Author

Montse Casas-Cabanas − *Centro de Investigación Cooperativa de Energías Alternativas (CIC energiGUNE), Basque Research and Technology Alliance (BRTA), 01510 Vitoria-Gasteiz, Spain; IKERBASQUE, Basque Foundation for Science, 48009 Bilbao, Spain;* orcid.org/0000-0002-9298-2333; Email: mcasas@cicenergigune.com

Authors

Marine Reynaud − *Centro de Investigación Cooperativa de Energías Alternativas (CIC energiGUNE), Basque Research and Technology Alliance (BRTA), 01510 Vitoria-Gasteiz, Spain;* orcid.org/0000-0002-0156-8701

Jon Serrano-Sevillano − *Centro de Investigación Cooperativa de Energías Alternativas (CIC energiGUNE), Basque*

https://doi.org/10.1021/acs.chemmater.2c03481
Chem. Mater. 2023, 35, 3345−3363

Research and Technology Alliance (BRTA), 01510 Vitoria-Gasteiz, Spain; orcid.org/0000-0003-1411-0270

Complete contact information is available at: https://pubs.acs.org/10.1021/acs.chemmater.2c03481

Author Contributions

[▽]These authors contributed equally. The manuscript was written through contributions of all authors. All authors have given approval to the final version of the manuscript.

Notes

The authors declare no competing financial interest.

Biographies

Marine Reynaud is associate researcher at CIC energiGUNE and leads a team dedicated to the design of new electrode and electrolyte materials. Having a dual expertise in inorganic synthesis and materials characterization, she has focused her research on understanding the correlations between composition, (micro)structure, and materials performance and on accelerating the development of new functional materials. In 2022, she was awarded a prize for her Research Projection from the Basque Research and Technology Alliance.

Jon Serrano Sevillano is a postdoctoral researcher at CIC energiGUNE. His research has been focused on the structural and electrochemical characterization of crystalline materials through a dual experimental and computational approach, with a special focus on defects. His expertise covers cathode and anode materials for Li-ion and Na-ion batteries.

Montse Casas-Cabanas is the scientific coordinator of the Electrochemical Energy Storage Area at CIC energiGUNE. Her research interests focus on the design of battery materials and the understanding of phenomena that occur in energy storage devices through a multidisciplinary approach, with a focus in crystal chemistry. She is the recipient of an Ikerbasque Research Associate Fellowship, and she has been recently awarded with the 2021 Young Researcher award from the Spanish Royal Society of Chemistry.

■ ACKNOWLEDGMENTS

The authors thank Iñigo Careaga for his help in the formatting of Figure [1]. This work was supported by the Spanish Ministry of Science and Innovation MCIN/AEI/10.13039/50110001103 through projects PID2019-107106RB-C33 and PID2019-106519RB-I00. M.C.C. also acknowledges Ikerbasque Science Foundation for a Research Associate position.

■ ABBREVIATIONS

APB, antiphase boundaries; BCDI, Bragg coherent diffractive imaging; BET, Brunauer−Emmett−Teller; EMD, electrolytic manganese dioxide; *fcc*, face-centered cubic; *hcp*, hexagonal close packed; ICE, initial Coulombic efficiency; Li-ion, lithium-ion; LNMO, lithium nickel manganese oxide; Na-ion, sodium-ion; NiCd batteries, nickel−cadmium batteries; NiMH batteries, nickel metal hydride batteries; ssNMR, solid-state nuclear magnetic resonance; NPD, neutron powder diffraction; PDF, pair distribution function; SAED, selected area electron diffraction; SG, space group; TEM, transmission electron microscopy; TM, transition metal(s); XRD, X-ray diffraction

■ REFERENCES

(1) Saremi, S.; Gao, R.; Dasgupta, A.; Martin, L. W. New Facets for the Role of Defects in Ceramics. *Am. Ceram. Soc. Bull.* **2018**, *97* (1), 16−23.

(2) Carter, C. B.; Norton, M. G. *Ceramic Materials: Science and Engineering*; Springer Science & Business Media, 2007.

(3) Shigley, J. E.; Breeding, C. M. Optical Defects in Diamond: A Quick Reference Chart. *Gems & Gemology* **2013**, *49* (2), 107−111.

(4) Abakumov, A. M.; Fedotov, S. S.; Antipov, E. v.; Tarascon, J.-M. Solid State Chemistry for Developing Better Metal-Ion Batteries. *Nat. Commun.* **2020**, *11* (1), 4976.

(5) Ohno, S.; Banik, A.; Dewald, G. F.; Kraft, M. A.; Krauskopf, T.; Minafra, N.; Till, P.; Weiss, M.; Zeier, W. G. Materials Design of Ionic Conductors for Solid State Batteries. *Progress in Energy* **2020**, *2* (2), 022001.

(6) Radin, M. D.; Hy, S.; Sina, M.; Fang, C.; Liu, H.; Vinckeviciute, J.; Zhang, M.; Whittingham, M. S.; Meng, Y. S.; van der Ven, A. Narrowing the Gap between Theoretical and Practical Capacities in Li-Ion Layered Oxide Cathode Materials. *Adv. Energy Mater.* **2017**, *7* (20), 1602888.

(7) Goodenough, J. B.; Kim, Y. Challenges for Rechargeable Li Batteries. *Chem. Mater.* **2010**, *22* (3), 587−603.

(8) Rousse, G.; Tarascon, J. M. Sulfate-Based Polyanionic Compounds for Li-Ion Batteries: Synthesis, Crystal Chemistry, and Electrochemistry Aspects. *Chem. Mater.* **2014**, *26* (1), 394−406.

(9) Hansen, N.; Barlow, C. Y. Plastic Deformation of Metals and Alloys. In *Physical Metallurgy*, 5th ed.; Laughlin, D. E., Hono, K., Eds.; Elsevier, 2014; pp 1681−1764 DOI: 10.1016/B978-0-444-53770-6.00017-4.

(10) Kaufman, J. L.; Vinckevičiūtė, J.; Kolli, S. K.; Goiri, J. G.; van der Ven, A. Understanding Intercalation Compounds for Sodium-Ion Batteries and Beyond. *Phil. Trans. R. Soc. A.* **2019**, *377* (2152), 20190020.

(11) Aguesse, F.; Manalastas, W.; Buannic, L.; Lopez del Amo, J. M.; Singh, G.; Llordés, A.; Kilner, J. Investigating the Dendritic Growth during Full Cell Cycling of Garnet Electrolyte in Direct Contact with Li Metal. *ACS Appl. Mater. Interfaces* **2017**, *9* (4), 3808−3816.

(12) Qin, Z.; Xie, Y.; Meng, X.; Qian, D.; Mao, D.; Zheng, Z.; Wan, L.; Huang, Y. Grain Boundary Engineering in Ta-Doped Garnet-Type Electrolyte for Lithium Dendrite Suppression. *ACS Appl. Mater. Interfaces* **2022**, *14* (36), 40959−40966.

(13) Morris, J. W., Jr. Defects in Crystals. In *Materials Science and Engineering: An Introduction*; Callister, W. D., Jr., Rethwisch, D. G., Eds.; Wiley, 2014; pp 76−107.

(14) Kittel, C. *Introduction to Solid State Physics*, 8th ed.; Wiley, 2004.

(15) Mohanty, D.; Li, J.; Abraham, D. P.; Huq, A.; Payzant, E. A.; Wood, D. L.; Daniel, C. Unraveling the Voltage-Fade Mechanism in High-Energy-Density Lithium-Ion Batteries: Origin of the Tetrahedral Cations for Spinel Conversion. *Chem. Mater.* **2014**, *26* (21), 6272−6280.

(16) Reed, J.; Ceder, G.; van der Ven, A. Layered-to-Spinel Phase Transition in Li_xMnO_2. *Electrochem. Solid-State Lett.* **2001**, *4*, A78.

(17) Liu, H.; Choe, M. J.; Enrique, R. A.; Orvañanos, B.; Zhou, L.; Liu, T.; Thornton, K.; Grey, C. P. Effects of Antisite Defects on Li Diffusion in $LiFePO_4$ Revealed by Li Isotope Exchange. *J. Phys. Chem. C* **2017**, *121* (22), 12025−12036.

(18) Hornbogen, E.; Petzow, G. Metallographie. *International Journal of Materials Research* **1970**, *61* (2), 81−94.

(19) Banerjee, A.; Wang, X.; Fang, C.; Wu, E. A.; Meng, Y. S. Interfaces and Interphases in All-Solid-State Batteries with Inorganic Solid Electrolytes. *Chem. Rev.* **2020**, *120* (14), 6878−6933.

(20) Casas-Cabanas, M.; Kim, C.; Rodríguez-Carvajal, J.; Cabana, J. Atomic Defects during Ordering Transitions in LiNi0.5Mn1.5O4 and Their Relationship with Electrochemical Properties. *J. Mater. Chem. A Mater.* **2016**, *4* (21), 8255−8262.

(21) Serrano-Sevillano, J.; Reynaud, M.; Saracibar, A.; Altantzis, T.; Bals, S.; van Tendeloo, G.; Casas-Cabanas, M. Enhanced Electrochemical Performance of Li-Rich Cathode Materials through Microstructural Control. *Phys. Chem. Chem. Phys.* **2018**, *20* (35), 23112−23122.

(22) Jarvis, K. A.; Deng, Z.; Allard, L. F.; Manthiram, A.; Ferreira, P. J. Understanding Structural Defects in Lithium-Rich Layered Oxide Cathodes. *J. Mater. Chem.* **2012**, *22* (23), 11550−11555.
(23) Bareño, J.; Balasubramanian, M.; Kang, S. H.; Wen, J. G.; Lei, C. H.; Pol, S. v.; Petrov, I.; Abraham, D. P. Long-Range and Local Structure in the Layered Oxide Li1.2Co 0.4Mn0.4O2. *Chem. Mater.* **2011**, *23* (8), 2039−2050.
(24) Wen, J. G.; Bareño, J.; Lei, C. H.; Kang, S. H.; Balasubramanian, M.; Petrov, I.; Abraham, D. P. Analytical Electron Microscopy of Li1.2Co0.4Mn 0.4O2 for Lithium-Ion Batteries. *Solid State Ion* **2011**, *182* (1), 98−107.
(25) Casas-Cabanas, M.; Reynaud, M.; Rikarte, J.; Horbach, P.; Rodríguez-Carvajal, J. FAULTS: A Program for Refinement of Structures with Extended Defects. *J. Appl. Crystallogr.* **2016**, *49* (6), 2259−2269.
(26) Chabre, Y.; Pannetier, J. Structural and Electrochemical Properties of the Proton/γ-MnO2 System. *Prog. Solid State Chem.* **1995**, *23* (1), 1−130.
(27) Shannon, R. D. Revised Effective Ionic Radii and Systematic Studies of Interatomic Distances in Halides and Chalcogenides. *Acta Crystallogr., Sect. A* **1976**, *32* (5), 751−767.
(28) Islam, M. S.; Driscoll, D. J.; Fisher, C. A. J.; Slater, P. R. Atomic-Scale Investigation of Defects, Dopants, and Lithium Transport in the $LiFePO_4$ Olivine-Type Battery Material. *Chem. Mater.* **2005**, *17* (20), 5085−5092.
(29) Malik, R.; Burch, D.; Bazant, M.; Ceder, G. Particle Size Dependence of the Ionic Diffusivity. *Nano Lett.* **2010**, *10* (10), 4123−4127.
(30) Rayavarapu, P. R.; Sharma, N.; Peterson, V. K.; Adams, S. Variation in Structure and Li + -Ion Migration in Argyrodite-Type Li 6PS 5X (X = Cl, Br, I) Solid Electrolytes. *J. Solid State Electrochem.* **2012**, *16*, 1807−1813.
(31) Deiseroth, H.-J.; Kong, S.-T.; Eckert, H.; Vannahme, J.; Reiner, C.; Zaiß, T.; Schlosser, M. Li6PS5X: A Class of Crystalline Li-Rich Solids With an Unusually High Li+ Mobility. *Angew. Chem., Int. Ed.* **2008**, *47* (4), 755−758.
(32) Kraft, M. A.; Ohno, S.; Zinkevich, T.; Koerver, R.; Culver, S. P.; Fuchs, T.; Senyshyn, A.; Indris, S.; Morgan, B. J.; Zeier, W. G. Inducing High Ionic Conductivity in the Lithium Superionic Argyrodites Li6+xP1-XGexS5I for All-Solid-State Batteries. *J. Am. Chem. Soc.* **2018**, *140* (47), 16330−16339.
(33) Kraft, M. A.; Culver, S. P.; Calderon, M.; Böcher, F.; Krauskopf, T.; Senyshyn, A.; Dietrich, C.; Zevalkink, A.; Janek, J.; Zeier, W. G. Influence of Lattice Polarizability on the Ionic Conductivity in the Lithium Superionic Argyrodites Li6PS5X (X = Cl, Br, I). *J. Am. Chem. Soc.* **2017**, *139* (31), 10909−10918.
(34) Hogrefe, K.; Minafra, N.; Hanghofer, I.; Banik, A.; Zeier, W. G.; Wilkening, H. M. R. Opening Diffusion Pathways through Site Disorder: The Interplay of Local Structure and Ion Dynamics in the Solid Electrolyte Li6+ XP1-XGexS5I as Probed by Neutron Diffraction and NMR. *J. Am. Chem. Soc.* **2022**, *144* (4), 1795−1812.
(35) Morgan, B. J. Mechanistic Origin of Superionic Lithium Diffusion in Anion-Disordered Li6PS5X Argyrodites. *Chem. Mater.* **2021**, *33* (6), 2004−2018.
(36) Stamminger, A. R.; Ziebarth, B.; Mrovec, M.; Hammerschmidt, T.; Drautz, R. Ionic Conductivity and Its Dependence on Structural Disorder in Halogenated Argyrodites Li6PS5X (X = Br, Cl, I). *Chem. Mater.* **2019**, *31*, 8673.
(37) de Klerk, N. J. J.; Rosłoń, I.; Wagemaker, M. Diffusion Mechanism of Li Argyrodite Solid Electrolytes for Li-Ion Batteries and Prediction of Optimized Halogen Doping: The Effect of Li Vacancies, Halogens, and Halogen Disorder. *Chem. Mater.* **2016**, *28* (21), 7955−7963.
(38) Gautam, A.; Sadowski, M.; Ghidiu, M.; Minafra, N.; Senyshyn, A.; Albe, K.; Zeier, W. G. Engineering the Site-Disorder and Lithium Distribution in the Lithium Superionic Argyrodite Li_6PS_5Br. *Adv. Energy Mater.* **2021**, *11* (5), 2003369.
(39) Fehse, M.; Etxebarria, N.; Otaegui, L.; Cabello, M.; Martín-Fuentes, S.; Cabañero, M. A.; Monterrubio, I.; Elkjær, C. F.; Fabelo, O.; Enkubari, N. A.; López Del Amo, J. M.; Casas-Cabanas, M.; Reynaud, M. Influence of Transition-Metal Order on the Reaction Mechanism of LNMO Cathode Spinel: An Operando X-Ray Absorption Spectroscopy Study. *Chem. Mater.* **2022**, *34* (14), 6529−6540.
(40) Cabana, J.; Casas-Cabanas, M.; Omenya, F. O.; Chernova, N. A.; Zeng, D.; Whittingham, M. S.; Grey, C. P. Composition-Structure Relationships in the Li-Ion Battery Electrode Material LiNi0.5Mn1.5O4e. *Chem. Mater.* **2012**, *24* (15), 2952−2964.
(41) Emery, N.; Bhatia, A.; Ghaleb, Y.; Mitrushchenkov, A. O.; Léonard, C.; Pereira-Ramos, J. P.; Baddour-Hadjean, R.; Smith, R. I. Short-Range to Long-Range Ni/Mn Order in $LiMn_2$-XNi XO_4($0.38 \leq x \leq 0.50$) Positive Electrode Materials: A Gradual Temperature-Driven Sublattice Disorder through Antiphase Boundary Defects. *Chem. Mater.* **2022**, *34* (7), 3152−3167.
(42) Delmas, C.; Fouassier, C.; Hagenmuller, P. Structural Classification and Properties of the Layered Oxides. *Physica B+C* **1980**, *99* (1−4), 81−85.
(43) Zeng, D.; Cabana, J.; Bréger, J.; Yoon, W. S.; Grey, C. P. Cation Ordering in Li[NixMnxCo(1−2x)] O2-Layered Cathode Materials: A Nuclear Magnetic Resonance (NMR), Pair Distribution Function, X-Ray Absorption Spectroscopy, and Electrochemical Study. *Chem. Mater.* **2007**, *19* (25), 6277−6289.
(44) Reynaud, M.; Casas-Cabanas, M. Order and Disorder in NMC Layered Materials: A FAULTS Simulation Analysis. *Powder Diffr* **2017**, *32* (S1), S213−S220.
(45) Xu, C.; Reeves, P. J.; Jacquet, Q.; Grey, C. P. Phase Behavior during Electrochemical Cycling of Ni-Rich Cathode Materials for Li-Ion Batteries. *Adv. Energy Mater.* **2021**, *11* (7), 2003404.
(46) Croguennec, L.; Pouillerie, C.; Mansour, A. N.; Delmas, C. Structural Characterisation of the Highly Deintercalated LixNi1.02O2 Phases (with $x \leq 0.30$). *J. Mater. Chem.* **2001**, *11* (1), 131−141.
(47) Gummow, R.; Thackeray, M.; David, W.; Hull, S. Structure and Electrochemistry of Lithium Cobalt Oxide Synthesised at 400°C. *Mater. Res. Bull.* **1992**, *27* (3), 327−337.
(48) Ohzuku, T.; Makimura, Y. Layered Lithium Insertion Material of LiNi 1/2 Mn 1/2 O 2 : A Possible Alternative to LiCoO 2 for Advanced Lithium-Ion Batteries. *Chem. Lett.* **2001**, *30* (8), 744−745.
(49) Kim, S.; Ma, X.; Ong, S. P.; Ceder, G. A Comparison of Destabilization Mechanisms of the Layered NaxMO2 and LixMO2 Compounds upon Alkali De-Intercalation. *Phys. Chem. Chem. Phys.* **2012**, *14* (44), 15571.
(50) Katcho, N. A.; Carrasco, J.; Saurel, D.; Gonzalo, E.; Han, M.; Aguesse, F.; Rojo, T. Origins of Bistability and Na Ion Mobility Difference in P2- and O3-$Na_{2/3}$ $Fe_{2/3}$ $Mn_{1/3}$ O_2 Cathode Polymorphs. *Adv. Energy Mater.* **2017**, *7* (1), 1601477.
(51) Takahashi, Y.; Gotoh, Y.; Akimoto, J. Single-Crystal Growth, Crystal and Electronic Structure of NaCoO2. *J. Solid State Chem.* **2003**, *172* (1), 22−26.
(52) Hasa, I.; Buchholz, D.; Passerini, S.; Hassoun, J. A Comparative Study of Layered Transition Metal Oxide Cathodes for Application in Sodium-Ion Battery. *ACS Appl. Mater. Interfaces* **2015**, *7* (9), 5206−5212.
(53) Ortiz-Vitoriano, N.; Drewett, N. E.; Gonzalo, E.; Acebedo, B.; Bonilla, F. J.; López del Amo, J. M.; Stansby, J. H.; Sharma, N.; Lakuntza, O.; Carrasco, J.; Rojo, T. High Performance P2 Sodium Layered Oxides: An in-Depth Study into the Effect of Rationally Selected Stoichiometry. *J. Mater. Chem. A Mater.* **2019**, *7* (38), 21812−21826.
(54) Berthelot, R.; Carlier, D.; Delmas, C. Electrochemical Investigation of the P2−NaxCoO2 Phase Diagram. *Nat. Mater.* **2011**, *10* (1), 74−80.
(55) Ouyang, B.; Chen, T.; Chen, X.; Fan, X.; Wang, J.; Liu, W.; Lu, Z.; Liu, K. Construction of Co/Ni-Free P2-Layered Metal Oxide Cathode with High Reversible Oxygen Redox for Sodium Ion Batteries. *Chemical Engineering Journal* **2023**, *452*, 138912.
(56) Wang, Y.; Xiao, R.; Hu, Y.-S.; Avdeev, M.; Chen, L. P2-Na0.6[Cr0.6Ti0.4]O2 Cation-Disordered Electrode for High-Rate

Symmetric Rechargeable Sodium-Ion Batteries. *Nat. Commun.* **2015**, *6* (1), 6954.
(57) Zhang, S.; Guo, Y.; Zhou, Y.; Zhang, X.; Niu, Y.; Wang, E.; Huang, L.; An, P.; Zhang, J.; Yang, X.; Yin, Y.; Xu, S.; Guo, Y. P3/O3 Integrated Layered Oxide as High-Power and Long-Life Cathode toward Na-Ion Batteries. *Small* **2021**, *17* (10), 2007236.
(58) Lei, Y.; Li, X.; Liu, L.; Ceder, G. Synthesis and Stoichiometry of Different Layered Sodium Cobalt Oxides. *Chem. Mater.* **2014**, *26* (18), 5288−5296.
(59) Didier, C.; Guignard, M.; Denage, C.; Szajwaj, O.; Ito, S.; Saadoune, I.; Darriet, J.; Delmas, C. Electrochemical Na-Deintercalation from NaVO2. *Electrochem. Solid-State Lett.* **2011**, *14* (5), A75.
(60) Arcelus, O.; Carrasco, J. Atomistic Insight into Glide-Driven Phase Transformations in Layered Oxides for Sodium-Ion Batteries: A Case Study on NaxVO2. *ACS Appl. Mater. Interfaces* **2019**, *11* (13), 12562−12569.
(61) Sathiya, M.; Jacquet, Q.; Doublet, M.-L.; Karakulina, O. M.; Hadermann, J.; Tarascon, J.-M. A Chemical Approach to Raise Cell Voltage and Suppress Phase Transition in O3 Sodium Layered Oxide Electrodes. *Adv. Energy Mater.* **2018**, *8* (11), 1702599.
(62) Silván, B.; Gonzalo, E.; Djuandhi, L.; Sharma, N.; Fauth, F.; Saurel, D. On the Dynamics of Transition Metal Migration and Its Impact on the Performance of Layered Oxides for Sodium-Ion Batteries: NaFeO 2 as a Case Study. *J. Mater. Chem. A Mater.* **2018**, *6* (31), 15132−15146.
(63) Somerville, J. W.; Sobkowiak, A.; Tapia-Ruiz, N.; Billaud, J.; Lozano, J. G.; House, R. A.; Gallington, L. C.; Ericsson, T.; Häggström, L.; Roberts, M. R.; Maitra, U.; Bruce, P. G. Nature of the "z"-Phase in Layered Na-Ion Battery Cathodes. *Energy Environ. Sci.* **2019**, *12* (7), 2223−2232.
(64) Rozier, P.; Tarascon, J. M. Review—Li-Rich Layered Oxide Cathodes for Next-Generation Li-Ion Batteries: Chances and Challenges. *J. Electrochem. Soc.* **2015**, *162* (14), A2490−A2499.
(65) Thackeray, M. M.; Johnson, C. S.; Vaughey, J. T.; Li, N.; Hackney, S. A. Advances in Manganese-Oxide "composite" Electrodes for Lithium-Ion Batteries. *J. Mater. Chem.* **2005**, *15* (23), 2257−2267.
(66) Thackeray, M. M.; Kang, S.-H.; Johnson, C. S.; Vaughey, J. T.; Hackney, S. A. Comments on the Structural Complexity of Lithium-Rich Li1+xM1−xO2 Electrodes (M = Mn, Ni, Co) for Lithium Batteries. *Electrochem commun* **2006**, *8* (9), 1531−1538.
(67) Thackeray, M. M.; Kang, S.-H.; Johnson, C. S.; Vaughey, J. T.; Benedek, R.; Hackney, S. A. Li2MnO3-Stabilized LiMO2 (M = Mn, Ni, Co) Electrodes for Lithium-Ion Batteries. *J. Mater. Chem.* **2007**, *17* (30), 3112.
(68) Croy, J. R.; Kim, D.; Balasubramanian, M.; Gallagher, K.; Kang, S.-H.; Thackeray, M. M. Countering the Voltage Decay in High Capacity XLi2MnO3·(1−x)LiMO2 Electrodes (M = Mn, Ni, Co) for Li+-Ion Batteries. *J. Electrochem. Soc.* **2012**, *159* (6), A781.
(69) Yu, H.; Ishikawa, R.; So, Y. G.; Shibata, N.; Kudo, T.; Zhou, H.; Ikuhara, Y. Direct Atomic-Resolution Observation of Two Phases in the Li 1.2Mn0.567Ni0.166Co0.067O 2 Cathode Material for Lithium-Ion Batteries. *Angewandte Chemie - International Edition* **2013**, *52* (23), 5969−5973.
(70) Lei, C. H.; Bareño, J.; Wen, J. G.; Petrov, I.; Kang, S. H.; Abraham, D. P. Local Structure and Composition Studies of Li1.2Ni0.2Mn0.6O2 by Analytical Electron Microscopy. *J. Power Sources* **2008**, *178* (1), 422−433.
(71) Lu, Z.; Dahn, J. R. Understanding the Anomalous Capacity of Li/Li[Ni[sub x]Li[sub (1/3−2x/3)]Mn[sub (2/3−x/3)]]O[sub 2] Cells Using In Situ X-Ray Diffraction and Electrochemical Studies. *J. Electrochem. Soc.* **2002**, *149*, A815.
(72) Lu, Z.; Chen, Z.; Dahn, J. R. Lack of Cation Clustering in Li[NixLi1/3-2x/3Mn2/3-x/3]O2 ($0 < x \leq 1/2$) and Li[CrxLi(1-x)/3Mn(2-2x)/3]O2 ($0 < x < 1$). *Chem. Mater.* **2003**, *15*, 3214−3220.
(73) Gu, M.; Belharouak, I.; Zheng, J.; Wu, H.; Xiao, J.; Genc, A.; Amine, K.; Thevuthasan, S.; Baer, D. R.; Zhang, J.-G.; Browning, N. D.; Liu, J.; Wang, C. Formation of the Spinel Phase in the Layered Composite Cathode Used in Li-Ion Batteries. *ACS Nano* **2013**, *7*, 760−767.
(74) Shukla, A. K.; Ramasse, Q. M.; Ophus, C.; Duncan, H.; Hage, F.; Chen, G. Unravelling structural ambiguities in lithium- and manganese-rich transition metal oxides. *Nat. Commun.* **2015**, *6*, 8711.
(75) Hu, S.; Pillai, A. S.; Liang, G.; Pang, W. K.; Wang, H.; Li, Q.; Guo, Z. Li-Rich Layered Oxides and Their Practical Challenges: Recent Progress and Perspectives. *Electrochemical Energy Reviews* **2019**, *2* (2), 277−311.
(76) Delmas, C. Battery Materials: Operating through Oxygen. *Nat. Chem.* **2016**, *8* (7), 641−643.
(77) Rozier, P.; Sathiya, M.; Paulraj, A. R.; Foix, D.; Desaunay, T.; Taberna, P. L.; Simon, P.; Tarascon, J. M. Anionic Redox Chemistry in Na-Rich Na2Ru1 - YSnyO3 Positive Electrode Material for Na-Ion Batteries. *Electrochem commun* **2015**, *53*, 29−32.
(78) Vinckeviciute, J.; Kitchaev, D. A.; van der Ven, A. A Two-Step Oxidation Mechanism Controlled by Mn Migration Explains the First-Cycle Activation Behavior of Li 2 MnO 3 -Based Li-Excess Materials. *Chem. Mater.* **2021**, *33* (5), 1625−1636.
(79) Kim, D.; Croy, J. R.; Thackeray, M. M. Comments on Stabilizing Layered Manganese Oxide Electrodes for Li Batteries. *Electrochem commun* **2013**, *36*, 103−106.
(80) Rinaldo, S. G.; Gallagher, K. G.; Long, B. R.; Croy, J. R.; Bettge, M.; Abraham, D. P.; Bareño, J.; Dees, D. W. Physical Theory of Voltage Fade in Lithium- and Manganese-Rich Transition Metal Oxides. *J. Electrochem. Soc.* **2015**, *162* (6), A897−A904.
(81) Chandan, P.; Chang, C. C.; Yeh, K. W.; Chiu, C. C.; Wu, D. Z.; Huang, T. W.; Wu, P. M.; Chi, P. W.; Hsu, W. F.; Su, K. H.; Lee, Y. W.; Chang, H. S.; Wang, M. J.; Wu, H. L.; Tang, H. Y.; Wu, M. K. Voltage Fade Mitigation in the Cationic Dominant Lithium-Rich NCM Cathode. *Commun. Chem.* **2019**, *2* (1), 1−7.
(82) Croy, J. R.; Balasubramanian, M.; Gallagher, K. G.; Burrell, A. K. Review of the U.S. Department of Energy's "Deep Dive" Effort to Understand Voltage Fade in Li- and Mn-Rich Cathodes. *Acc. Chem. Res.* **2015**, *48* (11), 2813−2821.
(83) Liu, J.; Hou, M.; Yi, J.; Guo, S.; Wang, C.; Xia, Y. Improving the Electrochemical Performance of Layered Lithium-Rich Transition-Metal Oxides by Controlling the Structural Defects. *Energy Environ. Sci.* **2014**, *7* (2), 705−714.
(84) Matsunaga, T.; Komatsu, H.; Shimoda, K.; Minato, T.; Yonemura, M.; Kamiyama, T.; Kobayashi, S.; Kato, T.; Hirayama, T.; Ikuhara, Y.; Arai, H.; Ukyo, Y.; Uchimoto, Y.; Ogumi, Z. Dependence of Structural Defects in Li2MnO3 on Synthesis Temperature. *Chem. Mater.* **2016**, *28* (12), 4143−4150.
(85) Menon, A. S.; Ojwang, D. O.; Willhammar, T.; Peterson, V. K.; Edström, K.; Gomez, C. P.; Brant, W. R. Influence of Synthesis Routes on the Crystallography, Morphology, and Electrochemistry of Li2MnO3. *ACS Appl. Mater. Interfaces* **2020**, *12* (5), 5939−5950.
(86) Lu, Z.; Beaulieu, L. Y.; Donaberger, R. A.; Thomas, C. L.; Dahn, J. R. Synthesis, Structure, and Electrochemical Behavior of Li[Ni[Sub x]Li[Sub 1/3−2x/3]Mn[Sub 2/3−x/3]]O[Sub 2]. *J. Electrochem. Soc.* **2002**, *149* (6), A778.
(87) Johnson, C. S.; Kim, J. S.; Lefief, C.; Li, N.; Vaughey, J. T.; Thackeray, M. M. The Significance of the Li 2MnO 3 Component in "composite" XLi 2MnO 3·(1 - x)LiMn 0.5Ni 0.5O 2 Electrodes. *Electrochem commun* **2004**, *6* (10), 1085−1091.
(88) Boulineau, A.; Croguennec, L.; Delmas, C.; Weill, F. Structure of Li2MnO3 with Different Degrees of Defects. *Solid State Ion* **2010**, *180* (40), 1652−1659.
(89) Seymour, I. D.; Middlemiss, D. S.; Halat, D. M.; Trease, N. M.; Pell, A. J.; Grey, C. P. Characterizing Oxygen Local Environments in Paramagnetic Battery Materials via 17O NMR and DFT Calculations. *J. Am. Chem. Soc.* **2016**, *138* (30), 9405−9408.
(90) Guerrini, N.; Jin, L.; Lozano, J. G.; Luo, K.; Sobkowiak, A.; Tsuruta, K.; Massel, F.; Duda, L. C.; Roberts, M. R.; Bruce, P. G. Charging Mechanism of Li2MnO3. *Chem. Mater.* **2020**, *32* (9), 3733−3740.
(91) Kang, S. H.; Kempgens, P.; Greenbaum, S.; Kropf, A. J.; Amine, K.; Thackeray, M. M. Interpreting the Structural and Electrochemical

https://doi.org/10.1021/acs.chemmater.2c03481
Chem. Mater. 2023, 35, 3345−3363

Complexity of 0.5Li2MnO3·0.5LiMO2 Electrodes for Lithium Batteries (M = Mn0.5-XNi0.5-XCo2x, 0 ≤ x≤ 0.5). *J. Mater. Chem.* **2007**, *17* (20), 2069−2077.
(92) Serrano-Sevillano, J.; Carlier, D.; Saracibar, A.; Lopez Del Amo, J. M.; Casas-Cabanas, M. DFT-Assisted Solid-State NMR Characterization of Defects in Li_2MnO_3. *Inorg. Chem.* **2019**, *58* (13), 8347−8356.
(93) Dogan, F.; Croy, J. R.; Balasubramanian, M.; Slater, M. D.; Iddir, H.; Johnson, C. S.; Vaughey, J. T.; Key, B. Solid State NMR Studies of Li 2 MnO 3 and Li-Rich Cathode Materials: Proton Insertion, Local Structure, and Voltage Fade. *J. Electrochem. Soc.* **2015**, *162* (1), A235−A243.
(94) Lee, Y. J.; Grey, C. P. Determining the Lithium Local Environments in the Lithium Manganates LiZn $_{0.5}$ Mn $_{1.5}$ O $_4$ and Li $_2$ MnO $_3$ by Analysis of the ^{6} Li MAS NMR Spinning Sideband Manifolds. *J. Phys. Chem. B* **2002**, *106* (14), 3576−3582.
(95) Boulineau, A.; Croguennec, L.; Delmas, C.; Weill, F. Reinvestigation of Li2MnO3 Structure: Electron Diffraction and High Resolution TEM. *Chem. Mater.* **2009**, *21* (18), 4216−4222.
(96) Boulineau, A.; Simonin, L.; Colin, J. F.; Canévet, E.; Daniel, L.; Patoux, S. Evolutions of Li 1.2Mn 0.61Ni 0.18Mg 0.01O 2 during the Initial Charge/Discharge Cycle Studied by Advanced Electron Microscopy. *Chem. Mater.* **2012**, *24* (18), 3558−3566.
(97) Coelho, A. A. *Topas Academic: General Profile and Structure Analysis Software for Powder Diffraction Data*; Bruker AXS: Karlsruhe, Germany, 2007.
(98) Casas-Cabanas, M.; Rodríguez-Carvajal, J.; Palacín, M. R. FAULTS, a New Program for Refinement of Powder Diffraction Patterns from Layered Structures. *Zeitschrift fur Kristallographie, Supplement* **2006**, *2006* (suppl_23_2006), 243−248.
(99) Treacy, M. M. J.; Newsam, J. M.; Deem, M. W. A General Recursion Method for Calculating Diffracted Intensities from Crystals Containing Planar Faults. *Proc. R Soc. Lond A Math Phys. Sci.* **1991**, *433* (1889), 499−520.
(100) Sun, Y.; Cong, H.; Zan, L.; Zhang, Y. Oxygen Vacancies and Stacking Faults Introduced by Low-Temperature Reduction Improve the Electrochemical Properties of Li_2MnO_3 Nanobelts as Lithium-Ion Battery Cathodes. *ACS Appl. Mater. Interfaces* **2017**, *9* (44), 38545−38555.
(101) Serrano-Sevillano, J.; Casas-Cabanas, M.; Saracibar, A. Impact of Stacking Faults and Li Substitution in LixMnO3 ($0 \leq x \leq 2$) Structural Transformations upon Delithiation. *J. Phys. Chem. Lett.* **2021**, *12*, 7474−7481.
(102) Mortemard de Boisse, B.; Reynaud, M.; Ma, J.; Kikkawa, J.; Nishimura, S.; Casas-Cabanas, M.; Delmas, C.; Okubo, M.; Yamada, A. Coulombic Self-Ordering upon Charging a Large-Capacity Layered Cathode Material for Rechargeable Batteries. *Nat. Commun.* **2019**, *10* (1), 2185.
(103) Yabuuchi, N.; Hara, R.; Kajiyama, M.; Kubota, K.; Ishigaki, T.; Hoshikawa, A.; Komaba, S. New O_2/P_2-Type Li-Excess Layered Manganese Oxides as Promising Multi-Functional Electrode Materials for Rechargeable Li/Na Batteries. *Adv. Energy Mater.* **2014**, *4*, 1301453.
(104) Qiao, Y.; Guo, S.; Zhu, K.; Liu, P.; Li, X.; Jiang, K.; Sun, C.-J.; Chen, M.; Zhou, H. Reversible Anionic Redox Activity in Na 3 RuO 4 Cathodes: A Prototype Na-Rich Layered Oxide. *Energy Environ. Sci.* **2018**, *11* (2), 299−305.
(105) Zhang, X.; Qiao, Y.; Guo, S.; Jiang, K.; Xu, S.; Xu, H.; Wang, P.; He, P.; Zhou, H. Manganese-Based Na-Rich Materials Boost Anionic Redox in High-Performance Layered Cathodes for Sodium-Ion Batteries. *Adv. Mater.* **2019**, *31* (27), 1807770.
(106) Liu, J.; Yin, L.; Wu, L.; Bai, J.; Bak, S.-M.; Yu, X.; Zhu, Y.; Yang, X.-Q.; Khalifah, P. G. Quantification of Honeycomb Number-Type Stacking Faults: Application to Na $_3$ Ni $_2$ BiO $_6$ Cathodes for Na-Ion Batteries. *Inorg. Chem.* **2016**, *55* (17), 8478−8492.
(107) Flamary-Mespoulie, F.; Boulineau, A.; Martinez, H.; Suchomel, M. R.; Delmas, C.; Pecquenard, B.; le Cras, F. Lithium-Rich Layered Titanium Sulfides: Cobalt- and Nickel-Free High Capacity Cathode Materials for Lithium-Ion Batteries. *Energy Storage Mater.* **2020**, *26*, 213−222.
(108) Viciu, L.; Huang, Q.; Morosan, E.; Zandbergen, H. W.; Greenbaum, N. I.; McQueen, T.; Cava, R. J. Structure and Basic Magnetic Properties of the Honeycomb Lattice Compounds Na2Co2TeO6 and Na3Co2SbO6. *J. Solid State Chem.* **2007**, *180* (3), 1060−1067.
(109) Masese, T.; Yoshii, K.; Kato, M.; Kubota, K.; Huang, Z. D.; Senoh, H.; Shikano, M. A High Voltage Honeycomb Layered Cathode Framework for Rechargeable Potassium-Ion Battery: P2-Type K2/3Ni1/3Co1/3Te1/3O2. *Chem. Commun.* **2019**, *55* (7), 985−988.
(110) Berthelot, R.; Schmidt, W.; Sleight, A. W.; Subramanian, M. A. Studies on Solid Solutions Based on Layered Honeycomb-Ordered Phases P2-Na 2M 2TeO 6 (M = Co, Ni, Zn). *J. Solid State Chem.* **2012**, *196*, 225−231.
(111) Berthelot, R.; Serrano-Sevillano, J.; Fraisse, B.; Fauth, F.; Weill, F.; Laurencin, D.; Casas-Cabanas, M.; Carlier, D.; Rousse, G.; Doublet, M.-L. Stacking Versatility in Alkali-Mixed Honeycomb Layered NaKNi 2 TeO 6. *Inorg. Chem.* **2021**, *60* (18), 14310−14317.
(112) Masese, T.; Miyazaki, Y.; Rizell, J.; Kanyolo, G. M.; Chen, C. Y.; Ubukata, H.; Kubota, K.; Sau, K.; Ikeshoji, T.; Huang, Z. D.; Yoshii, K.; Takahashi, T.; Ito, M.; Senoh, H.; Hwang, J.; Alshehabi, A.; Matsumoto, K.; Matsunaga, T.; Fujii, K.; Yashima, M.; Shikano, M.; Tassel, C.; Kageyama, H.; Uchimoto, Y.; Hagiwara, R.; Saito, T. Mixed Alkali-Ion Transport and Storage in Atomic-Disordered Honeycomb Layered NaKNi2TeO6. *Nat. Commun.* **2021**, *12* (1), 1−16.
(113) Masese, T.; Yoshii, K.; Yamaguchi, Y.; Okumura, T.; Huang, Z. D.; Kato, M.; Kubota, K.; Furutani, J.; Orikasa, Y.; Senoh, H.; Sakaebe, H.; Shikano, M. Rechargeable Potassium-Ion Batteries with Honeycomb-Layered Tellurates as High Voltage Cathodes and Fast Potassium-Ion Conductors. *Nat. Commun.* **2018**, *9* (1), 1−12.
(114) Casas-Cabanas, M.; Canales-Vázquez, J.; Rodríguez-Carvajal, J.; Palacín, M. R. Deciphering the Structural Transformations during Nickel Oxyhydroxide Electrode Operation. *J. Am. Chem. Soc.* **2007**, *129* (18), 5840−5842.
(115) Casas-Cabanas, M.; Radin, M. D.; Kim, J.; Grey, C. P.; van der Ven, A.; Palacín, M. R. The Nickel Battery Positive Electrode Revisited: Stability and Structure of the β-NiOOH Phase. *J. Mater. Chem. A Mater.* **2018**, *6* (39), 19256−19265.
(116) Oliva, P.; Leonardi, J.; Laurent, J. F.; Delmas, C.; Braconnier, J. J.; Figlarz, M.; Fievet, F.; Guibert, A. de. Review of the Structure and the Electrochemistry of Nickel Hydroxides and Oxy-Hydroxides. *J. Power Sources* **1982**, *8* (2), 229−255.
(117) Casas-Cabanas, M.; Palacín, M. R.; Rodríguez-Carvajal, J. Microstructural Analysis of Nickel Hydroxide: Anisotropic Size versus Stacking Faults. *Powder Diffr* **2005**, *20* (4), 334−344.
(118) Delmas, C.; Tessier, C. Stacking Faults in the Structure of Nickel Hydroxide: A Rationale of Its High Electrochemical Activity. *J. Mater. Chem.* **1997**, *7* (8), 1439−1443.
(119) Tessier, C.; Haumesser, P. H.; Bernard, P.; Delmas, C. The Structure of Ni (OH) 2: From the Ideal Material to the Electrochemically Active One. *J. Electrochem. Soc.* **1999**, *146* (6), 2059−2067.
(120) Wronski, Z. S.; Carpenter, G. J. C.; Kalal, P. J.An Integrated Characterization Approach for Ranking Ni Hydroxides Designed for High-Performance Positive Electrodes in Batteries for Electric Vehicles. In *Proceedings of the Symposium on Exploratory Research and Development of Batteries for Electric and Hybrid Vehicles*; Adams, W. A., Landgrebe, A. R., Scrosati, B., Eds.; Proceedings, Vol. *96-14*; The Electrochemical Society, Inc.: Pennington, NJ, 1996; pp 177−188.
(121) Casas-Cabanas, M.; Rodríguez-Carvajal, J.; Canales-Vázquez, J.; Palacín, M. R. New Insights on the Microstructural Characterisation of Nickel Hydroxides and Correlation with Electrochemical Properties. *J. Mater. Chem.* **2006**, *16* (28), 2925−2939.
(122) Asenbauer, J.; Eisenmann, T.; Kuenzel, M.; Kazzazi, A.; Chen, Z.; Bresser, D. The Success Story of Graphite as a Lithium-Ion Anode

https://doi.org/10.1021/acs.chemmater.2c03481
Chem. Mater. 2023, 35, 3345−3363

Material-Fundamentals, Remaining Challenges, and Recent Developments Including Silicon (Oxide) Composites. *Sustain Energy Fuels* **2020**, *4* (11), 5387−5416.
(123) Franklin, R. E. Crystallite Growth in Graphitizing and Non-Graphitizing Carbons. *Proc. R Soc. Lond A Math Phys. Sci.* **1951**, *209* (1097), 196−218.
(124) Herstedt, M.; Fransson, L.; Edström, K. Rate Capability of Natural Swedish Graphite as Anode Material in Li-Ion Batteries. *J. Power Sources* **2003**, *124* (1), 191−196.
(125) Dittrich, H.; Wohlfahrt-Mehrens, M. Stacking Fault Analysis in Layered Materials. *International Journal of Inorganic Materials* **2001**, *3* (8), 1137−1142.
(126) Shi, H.; Barker, J.; Saïdi, M. Y.; Koksbang, R. Structure and Lithium Intercalation Properties of Synthetic and Natural Graphite. *J. Electrochem. Soc.* **1996**, *143* (11), 3466−3472.
(127) Shi, H.; Barker, J.; Saïdi, M. Y.; Koksbang, R.; Morris, L. Graphite Structure and Lithium Intercalation. *J. Power Sources* **1997**, *68* (2), 291−295.
(128) Zheng, T.; Reimers, J. N.; Dahn, J. R. Effect of Turbostratic Disorder in Graphitic Carbon Hosts on the Intercalation of Lithium. *Phys. Rev. B* **1995**, *51* (2), 734−741.
(129) Chen, Z.; Qin, Y.; Ren, Y.; Lu, W.; Orendorff, C.; Roth, E. P.; Amine, K. Multi-Scale Study of Thermal Stability of Lithiated Graphite. *Energy Environ. Sci.* **2011**, *4* (10), 4023−4030.
(130) Black, A. P.; Torres, A.; Frontera, C.; Palacín, M. R.; Arroyo-De Dompablo, M. E. Appraisal of Calcium Ferrites as Cathodes for Calcium Rechargeable Batteries: DFT, Synthesis, Characterization and Electrochemistry of Ca4Fe9O17. *Dalton Transactions* **2020**, *49* (8), 2671−2679.
(131) Malaman, B.; Alebouyeh, H.; Courtois, A.; Gérardin, R.; Evrard, O. La Structure Cristalline de Ca4Fe9O17: Des Feuillets "Hexagonaux" d'octaedres FeO6 et de Bipyramides FeO5 Lies Par Des Tetraedres FeO4. *Mater. Res. Bull.* **1982**, *17* (6), 795−800.
(132) Serrano-Sevillano, J.; Oró-Solé, J.; Gázquez, J.; Frontera, C.; Black, A. P.; Casas-Cabanas, M.; Palacín, M. R. Assessing the Local Structure and Quantifying Defects in Ca 4 Fe 9 O 17 Combining STEM and FAULTS. *Inorg. Chem. Front* **2022**, *9* (24), 6425−6430.
(133) Asano, T.; Sakai, A.; Ouchi, S.; Sakaida, M.; Miyazaki, A.; Hasegawa, S. Solid Halide Electrolytes with High Lithium-Ion Conductivity for Application in 4 V Class Bulk-Type All-Solid-State Batteries. *Adv. Mater.* **2018**, *30* (44), 1803075.
(134) Li, X.; Liang, J.; Yang, X.; Adair, K. R.; Wang, C.; Zhao, F.; Sun, X. Progress and Perspectives on Halide Lithium Conductors for All-Solid-State Lithium Batteries. *Energy Environ. Sci.* **2020**, *13* (5), 1429−1461.
(135) Wan, T. H.; Ciucci, F. Ab Initio Study of the Defect Chemistry and Substitutional Strategies for Highly Conductive Li3YX6(X = F, Cl, Br, and I) Electrolyte for the Application of Solid-State Batteries. *ACS Appl. Energy Mater.* **2021**, *4* (8), 7930−7941.
(136) Li, X.; Liang, J.; Adair, K. R.; Li, J.; Li, W.; Zhao, F.; Hu, Y.; Sham, T. K.; Zhang, L.; Zhao, S.; Lu, S.; Huang, H.; Li, R.; Chen, N.; Sun, X. Origin of Superionic $Li_3Y_{1-x}In_xCl_6$ Halide Solid Electrolytes with High Humidity Tolerance. *Nano Lett.* **2020**, *20* (6), 4384−4392.
(137) Wu, E. A.; Banerjee, S.; Tang, H.; Richardson, P. M.; Doux, J. M.; Qi, J.; Zhu, Z.; Grenier, A.; Li, Y.; Zhao, E.; Deysher, G.; Sebti, E.; Nguyen, H.; Stephens, R.; Verbist, G.; Chapman, K. W.; Clément, R. J.; Banerjee, A.; Meng, Y. S.; Ong, S. P. A Stable Cathode-Solid Electrolyte Composite for High-Voltage, Long-Cycle-Life Solid-State Sodium-Ion Batteries. *Nat. Commun.* **2021**, *12*, 1256 DOI: 10.1038/s41467-021-21488-7.
(138) Liang, J.; Li, X.; Wang, S.; Adair, K. R.; Li, W.; Zhao, Y.; Wang, C.; Hu, Y.; Zhang, L.; Zhao, S.; Lu, S.; Huang, H.; Li, R.; Mo, Y.; Sun, X. Site-Occupation-Tuned Superionic LixScCl3+ XHalide Solid Electrolytes for All-Solid-State Batteries. *J. Am. Chem. Soc.* **2020**, *142* (15), 7012−7022.
(139) Plass, M. A.; Bette, S.; Dinnebier, R. E.; Lotsch, B. v. Enhancement of Superionic Conductivity by Halide Substitution in Strongly Stacking Faulted Li3HoBr6- XIxPhases. *Chem. Mater.* **2022**, *34* (7), 3227−3235.
(140) Sebti, E.; Evans, H. A.; Chen, H.; Richardson, P. M.; White, K. M.; Giovine, R.; Koirala, K. P.; Xu, Y.; Gonzalez-Correa, E.; Wang, C.; Brown, C. M.; Cheetham, A. K.; Canepa, P.; Clément, R. J. Stacking Faults Assist Lithium-Ion Conduction in a Halide-Based Superionic Conductor. *J. Am. Chem. Soc.* **2022**, *144* (13), 5795−5811.
(141) Schlem, R.; Muy, S.; Prinz, N.; Banik, A.; Shao-Horn, Y.; Zobel, M.; Zeier, W. G. Mechanochemical Synthesis: A Tool to Tune Cation Site Disorder and Ionic Transport Properties of Li_3MCl_6 (M = Y, Er) Superionic Conductors. *Adv. Energy Mater.* **2020**, *10* (6), 1903719.
(142) Ito, H.; Shitara, K.; Wang, Y.; Fujii, K.; Yashima, M.; Goto, Y.; Moriyoshi, C.; Rosero-Navarro, N. C.; Miura, A.; Tadanaga, K. Kinetically Stabilized Cation Arrangement in Li_3YCl_6 Superionic Conductor during Solid-State Reaction. *Advanced Science* **2021**, *8* (15), 2101413.
(143) de Wolff, P. M.; Visser, J. W.; Giovanoli, R.; Brutsch, R. Epsilon Manganese Dioxide. *Chimia* **1978**, *32* (7), 257−259.
(144) de Wolff, P. M. Interpretation of Some γ-MnO 2 Diffraction Patterns. *Acta Crystallogr.* **1959**, *12* (4), 341−345.
(145) Preisler, E. Growth of Electrodeposited ?-Manganese Dioxide from a Suspension Bath. *J. Appl. Electrochem.* **1989**, *19* (4), 540−546.
(146) Andersen, T. Effect of Some EMD Structural Features on Alkaline Discharge Capacity. In *Progress in Batteries and Battery Materials*, Vol *11*; Ite-Jec Press: Brunswick, OH, 1992; pp 105−129.
(147) Williams, R.; Fredlein, R.; Lawrence, G.; Swinkels, D. A. J. Effect of Deposition Conditions on the Structural, Chemical, Physical and Electrochemical Properties of EMD In *Progress in Batteries and Battery Materials*, Vol *13*; Ite-Jec Press: Brunswick, OH, 1994; pp 102−112.
(148) Simon, D. E.; Morton, R. W.; Gislason, J. J. A CLOSE LOOK AT ELECTROLYTIC MANGANESE DIOXIDE (EMD) AND THE γ-MnO_2 & ε-MnO_2 PHASES USING RIETVELD MODELING. *Adv. X-ray Anal.* **2003**, *47*, 267−280.
(149) Magnard, N. P. L.; Anker, A. S.; Aalling-Frederiksen, O.; Kirsch, A.; Jensen, K. M. Ø. Characterisation of Intergrowth in Metal Oxide Materials Using Structure-Mining: The Case of γ-MnO_2. *Dalton Trans.* **2022**, *51*, 17150−17161.
(150) Galliez, K.; Deniard, P.; Petit, P.-E.; Lambertin, D.; Bart, F.; Jobic, S. Modelling and Quantification of Intergrowth in γ-MnO 2 by Laboratory Pair Distribution Function Analysis. *J. Appl. Crystallogr.* **2014**, *47* (2), 552−560.
(151) McCalla, E.; Abakumov, A.; Rousse, G.; Reynaud, M.; Sougrati, M. T.; Budic, B.; Mahmoud, A.; Dominko, R.; van Tendeloo, G.; Hermann, R. P.; Tarascon, J. M. Novel Complex Stacking of Fully-Ordered Transition Metal Layers in Li_4FeSbO_6 Materials. *Chem. Mater.* **2015**, *27* (5), 1699−1708.
(152) Peng, S.; Chen, Y.; Wang, B.; Zhou, X.; Yu, H.; Wang, J.; Yang, W.; Gao, X. Intrinsic Layered Defects in Solid-State Electrolyte Li0.33La0.56TiO3. *Mater. Today Energy* **2022**, *23*, 100912.
(153) Scholz, T.; Schneider, C.; Eger, R.; Duppel, V.; Moudrakovski, I.; Schulz, A.; Nuss, J.; Lotsch, B. v. Phase Formation through Synthetic Control: Polymorphism in the Sodium-Ion Solid Electrolyte Na4P2S6. *J. Mater. Chem. A Mater.* **2021**, *9* (13), 8692−8703.
(154) Moriwake, H.; Kuwabara, A.; Fisher, C. A. J.; Huang, R.; Hitosugi, T.; Ikuhara, Y. H.; Oki, H.; Ikuhara, Y. First-Principles Calculations of Lithium-Ion Migration at a Coherent Grain Boundary in a Cathode Material, LiCoO 2. *Adv. Mater.* **2013**, *25* (4), 618−622.
(155) Wang, C.; Wang, S.; He, Y.-B.; Tang, L.; Han, C.; Yang, C.; Wagemaker, M.; Li, B.; Yang, Q.-H.; Kim, J.-K.; Kang, F. Combining Fast Li-Ion Battery Cycling with Large Volumetric Energy Density: Grain Boundary Induced High Electronic and Ionic Conductivity in Li 4 Ti 5 O 12 Spheres of Densely Packed Nanocrystallites. *Chem. Mater.* **2015**, *27* (16), 5647−5656.
(156) Gabrisch, H.; Yazami, R.; Fultz, B. The Character of Dislocations in LiCoO[Sub 2]. *Electrochem. Solid-State Lett.* **2002**, *5* (6), A111.

(157) Dresselhaus, M. S.; Dresselhaus, G. Intercalation Compounds of Graphite. *Adv. Phys.* **1981**, *30* (2), 139−326.
(158) Cherns, D.; Ngo, G. P. Electron Microscope Studies of Sodium and Lithium Intercalation in TiS2. *J. Solid State Chem.* **1983**, *50* (1), 7−19.
(159) Ulvestad, A.; Singer, A.; Clark, J. N.; Cho, H. M.; Kim, J. W.; Harder, R.; Maser, J.; Meng, Y. S.; Shpyrko, O. G. Topological Defect Dynamics in Operando Battery Nanoparticles. *Science (1979)* **2015**, *348* (6241), 1344−1347.
(160) Singer, A.; Zhang, M.; Hy, S.; Cela, D.; Fang, C.; Wynn, T. A.; Qiu, B.; Xia, Y.; Liu, Z.; Ulvestad, A.; Hua, N.; Wingert, J.; Liu, H.; Sprung, M.; Zozulya, A. v.; Maxey, E.; Harder, R.; Meng, Y. S.; Shpyrko, O. G. Nucleation of Dislocations and Their Dynamics in Layered Oxide Cathode Materials during Battery Charging. *Nat. Energy* **2018**, *3* (8), 641−647.
(161) Legros, M.; Dehm, G.; Arzt, E.; Balk, T. J. Observation of Giant Diffusivity Along Dislocation Cores. *Science (1979)* **2008**, *319* (5870), 1646−1649.
(162) Strange, J. H.; Rageb, S. M.; Slade, R. C. T. Investigation of Ionic Transport in Composites by Nuclear Magnetic Resonance. *Philosophical Magazine A* **1991**, *64* (5), 1159−1166.
(163) Goiri, J. G.; van der Ven, A. MultiShifter: Software to Generate Structural Models of Extended Two-Dimensional Defects in 3D and 2D Crystals. *Comput. Mater. Sci.* **2021**, *191*, 110310.
(164) Maier, J. Review—Battery Materials: Why Defect Chemistry? *J. Electrochem. Soc.* **2015**, *162* (14), A2380−A2386.

https://doi.org/10.1021/acs.chemmater.2c03481
Chem. Mater. 2023, 35, 3345−3363